




AcRR1 of *Agropyron cristatum* boosts wheat yield by regulating grain number per spike and heading date

Received: 16 October 2024

Accepted: 7 July 2025

Published online: 18 July 2025



Wenjing Yang^{1,5}, Haiming Han^{1,5} , Huihui Ma^{2,5}, Ping Yang¹, Jianqing Niu³, Xinye Liu⁴, Jinpeng Zhang¹, Shenghui Zhou¹, Kai Qi¹, Baojin Guo¹, Yida Lin³, Xinming Yang¹, Xiaomin Guo³, Hong-Qing Ling³  & Lihui Li^{1,3} 

Uncovering desirable alien genes from wild species is important for increasing genetic variation and ensuring wheat production. Here, we identify a type-B response regulator (RR) *AcRR1* of *Agropyron cristatum*. Ectopic expression of *AcRR1* in common wheat increases the grain number per spike without decreasing the grain weight, thereby enhancing the grain yield by 9.7–12.3% under field conditions. Expression of the *AcRR1* gene also promotes plant growth and shortens the duration of vernalization in the transgenic plants. We reveal that *AcRR1* reprogrammes diverse transcriptional processes in wheat by activating the expression of *TaWOX11-2D* and *TabHLH25-5B-TaFTs*, which are involved in floret fertility and early heading. Our results demonstrate that *AcRR1* from *A. cristatum* is a valuable alien gene with the capacity to activate genetic networks for wheat yield formation, offering a promising avenue for enhancing wheat productivity through the introduction of alien genes.

Common wheat (*Triticum aestivum* L., AABBDD, $2n = 6x = 42$), a staple food crop, is one of the most important cereal crops in the world, with a planting area of more than 220 million hectares and an annual output of more than 620 million tons (FAOSTAT 2024), providing nearly 20% of the protein and calories in the world¹. Constant improvements in wheat grain yield are essential for global food security. Wheat yield consists of three major components: spike number per unit area, grain number per spike (GNS), and grain weight^{2,3}. During the past 50 years, wheat yield has greatly improved, e.g., the average wheat yield in China increased from 1840.5 kg/ha in 1978 to 5740.5 kg/ha in 2021⁴. The improvement in yield is attributable mainly to the use of dwarf and semidwarf alleles of *Rht* loci, resulting in a reduced plant height, increased plant density and spike number per unit area, and elevated harvest index and lodging resistance⁴. When the spike number per unit area reaches a certain level, increasing the GNS seems to be a more

effective way to increase the wheat yield. The GNS comprises the spikelet number per spike and the grain number per spikelet⁵. The grain number per spikelet is further determined by the number of florets per spikelet, the number of degraded florets per spikelet and the seed setting rate^{5,6}. Each wheat spikelet usually produces up to 12 floret primordia. However, more than 70% of the florets abort during their development, and only the bottom 1–4 florets of each spikelet develop and become fertilized^{7,8}. Therefore, reducing floret abortion and enhancing floret fertility are important strategies for increasing the GNS and improving wheat yield.

Usually, the GNS and grain weight are negatively correlated in wheat and other cereal crops⁹. Identifying a gene(s) that can balance the GNS and grain weight and even disrupt this negative correlation is a major challenge for crop scientists and breeders. In rice, the genes *IPA1*¹⁰, *GY3*¹¹, *OsMADS17*¹² and *OsDREB1C*¹³ can balance the GNS and

¹State Key Laboratory of Crop Gene Resources and Breeding, Key Laboratory of Grain Crop Genetic Resources Evaluation and Utilization, Institute of Crop Sciences, Chinese Academy of Agricultural Sciences, Beijing, China. ²College of Life Sciences, Zaozhuang University, Zaozhuang, China. ³Yazhouwan National Laboratory, Sanya, China. ⁴Ministry of Education Key Laboratory of Molecular and Cellular Biology, Hebei Collaboration Innovation Center for Cell Signaling and Environmental Adaptation, Hebei Key Laboratory of Molecular and Cellular Biology, College of Life Sciences, Hebei Normal University, Shijiazhuang, China. ⁵These authors contributed equally: Wenjing Yang, Haiming Han, Huihui Ma. ✉ e-mail: hanhaiming@caas.cn; hqling@genetics.ac.cn; lilihui@caas.cn

grain weight well. However, the identification of such genes in wheat is still limited. Wolde et al.³ reported that the genetic modification of spikelet arrangement via introgression of the *bht-A1* allele into durum wheat increased the grain number without affecting the grain weight. Additionally, mutation of *grain number increase 1* (*GNI1*) in wheat resulted in increases in the number of fertile florets per spikelet and the number of grains per spike without negative effects on grain weight⁸.

Heading date is also a critical determinant enabling crops to adapt to climate change and make maximum use of the temperature and sunlight that are available under specific ecological conditions¹⁴. However, early heading and maturity are accompanied by a shortened growth cycle and reduced biomass accumulation in crops, leading to a yield penalty¹⁵. Tackling the intricate trade-offs among various traits can facilitate plant breeding to overcome yield plateaus, which requires an exploration of pioneering genetic reservoirs sourced from a wealthy germplasm resource. Therefore, the trade-off between grain yield and heading date (maturity) is important for wheat improvement.

Wild relatives of wheat provide a valuable source of genes and allelic variants for wheat improvement^{16,17}. Remarkable progress has been made in the utilization of wild relatives in wheat breeding^{4,18}. *Agropyron cristatum* (PPPP, $2n = 4x = 28$) is a wild relative of wheat that possesses considerable genetic diversity for improving wheat traits, such as spikelets, florets, fertile tillers, and resistance to certain diseases and abiotic stresses^{19,20}. Some desirable genes from *A. cristatum* have been introduced into common wheat via distant hybridization^{21–27}. Chromosome 6P of *A. cristatum* has been confirmed to harbor genes that substantially increase the GNS in wheat²¹. The wheat–*A. cristatum* 6P addition line 5113 presented a significant increase in the GNS. A series of 6P translocation lines derived from addition lines have been developed and serve as desirable germplasm resources for wheat breeding^{28,29}.

In this study, we show that a type-B response regulator (RR) *AcRR1* originated from *A. cristatum* increases GNS and grain yield but reduces growth and vernalization duration through the coordination with *TaWOX11-2D* and *TabHLH25-5B–TaFT-B1* pathways. This work reveals an alien gene valuable for high-yield wheat breeding and serves as an example for broadening the genetic diversity of wheat via the use of alien genes from its wild relatives.

Results

Identification of *AcRR1*

In our previous studies, a pair of wheat–*A. cristatum* 6P addition lines, 5113³⁰ and II-30-5³¹, were generated via distant hybridization between the *T. aestivum* cultivar (cv.) Fukuohokomugi (Fukuho hereafter) and *A. cristatum* accession Z559. Compared with Fukuho, the addition line 5113 presented a drastic increase in the GNS of 26.0 grains, whereas the addition line II-30-5, which carried a different 6P chromosome, did not show an increase in the GNS (Fig. 1a–c). We generated two wheat–*A. cristatum* 6P translocation lines, WAT63b and WAT65b, by irradiating the addition line 5113 and backcrossing with Fukuho for three generations to transfer the fruitful GNS trait to common wheat. GISH analysis and genome resequencing revealed that WAT63b is a T6PL-6PS-5BL translocation line, in which the short arm and part of the long arm of chromosome 5B were replaced by the long arm plus 53% of the short arm (6PS: 0.00–0.53) of *A. cristatum* 6P, whereas WAT65b is a T6PL-6PS-5AS translocation line, in which the long arm and part of the short arm of chromosome 5A were replaced by the long arm plus 22% of the short arm (6PS: 0.00–0.22) of *A. cristatum* 6P (Fig. 1d and Supplementary Fig. 1a–d). Phenotypic characterization revealed that, compared with the recipient parent Fukuho, the number of grains per spike of WAT63b increased by 10.0 grains, while that of WAT65b did not (Fig. 1e–g). Further analysis revealed that the increased GNS in WAT63b was attributable mainly to an increased grain number per spikelet. Owing to the difference in translocated chromosome length

between WAT63b (6PS: 0.00–0.53) and WAT65b (6PS: 0.00–0.22) in the short arm of *A. cristatum* 6P, the underlying gene(s) of the fruitful GNS were delimited to the 6PS bin 0.22–0.53 (Fig. 1d). The clean reads of the WAT63b and WAT65b resequencing data were mapped to the genome assembly of *A. cristatum* Z559³² and Chinese Spring RefSeqv2.1³³ to further identify the translocated chromosomal segment. As shown in Supplementary Fig. 1c, the different lengths of the translocated 6PS segment between WAT63b and WAT65b were determined to be 155.0–355.0 Mb for *A. cristatum* 6P, which contains 1252 predicted genes.

To identify the candidate gene(s) responsible for increased GNS, we performed a transcriptome analysis with the wheat–*A. cristatum* 6P addition lines 5113 and II-30-5³⁴. The comparative analysis revealed that a total of 150 genes were significantly differentially expressed in bins 0.22–0.53 of the 6PS between 5113 and II-30-5, including 149 upregulated genes and one downregulated gene (Fig. 1h and Supplementary Data 1). Among these genes, seven were annotated to be involved in plant growth and development. We then conducted a comparative analysis of the spatiotemporal expression patterns of the seven genes between addition lines 5113 and II-30-5 during young spike differentiation (Supplementary Fig. 1e–j). Among these genes, *Ac6P01G257700* and *Ac6P01G234400*, which encode type-B RR and SWI/SNF chromatin-remodeling complex subunit SWI3B, respectively, were expressed at significantly higher levels in 5113 than in II-30-5, especially during the young inflorescence development and floret abortion stages (Fig. 1i). The type-B RR is an important component of the cytokinin signaling pathway^{35,36}, which is strongly associated with meristem development and grain yield^{37,38}. We further conducted a haplotype analysis of the wheat orthologs of *Ac6P01G257700* using a population containing 355 wheat accessions worldwide³⁹. The variants (SNPs and InDels ≤ 8 bp) in the homologous genes of *Ac6P01G257700* (from 2 kb upstream of ATG to 500 bp downstream of TAG) were used to classify the haplotypes. As shown in Supplementary Fig. 2, the superior haplotype Hap_Alt of its homologous gene on chromosome 6A (*TaRR1-6A*) and Hap4 of its homologous gene on chromosome 6B (*TaRR1-6B*) presented significant increases in the grain number per spike and grain number per spikelet, whereas the superior haplotype Hap_CS of the homologous gene on chromosome 6D (*TaRR1-6D*) presented increases in the spikelet number per spike and grain number per spike compared with the inferior haplotype. These results implied that the wheat orthologs of *Ac6P01G257700* function in the regulation of grain number per spike. Therefore, we selected *Ac6P01G257700* as the candidate gene for further investigation and named it *AcRR1*.

AcRR1 possesses six exons and five introns (Fig. 1j). It encodes a type-B RR protein containing a conserved MYB-like DNA binding domain and a signal receiver domain (Supplementary Fig. 3a). Transient expression assays in wheat protoplasts revealed that the *AcRR1*-GFP fusion protein was localized exclusively in the nucleus (Supplementary Fig. 3b), suggesting that *AcRR1* may function as a transcription factor. We performed a transcriptional activation assay in yeast cells to confirm this hypothesis, and the results showed that *AcRR1* indeed possessed transcriptional activation activity (Supplementary Fig. 3c). Phylogenetic analysis revealed that *AcRR1* was evolutionarily close to its barley and wheat orthologs and showed some sequence divergence from its wheat orthologs (Supplementary Fig. 3d, e and Supplementary Fig. 4).

The expression of *AcRR1* in common wheat increases GNS and yield

To study the genetic effect of *AcRR1* in wheat, the coding sequence (CDS) of *AcRR1* driven by the ubiquitin promoter of maize (*Zea mays* L.) was introduced into the spring wheat cv. Fielder by *Agrobacterium*-mediated transformation, and five independent transgenic lines were generated. In accordance with the transcriptional abundance of *AcRR1* (Supplementary Fig. 5a), the transgenic *AcRR1*-OE1, *AcRR1*-OE3 and

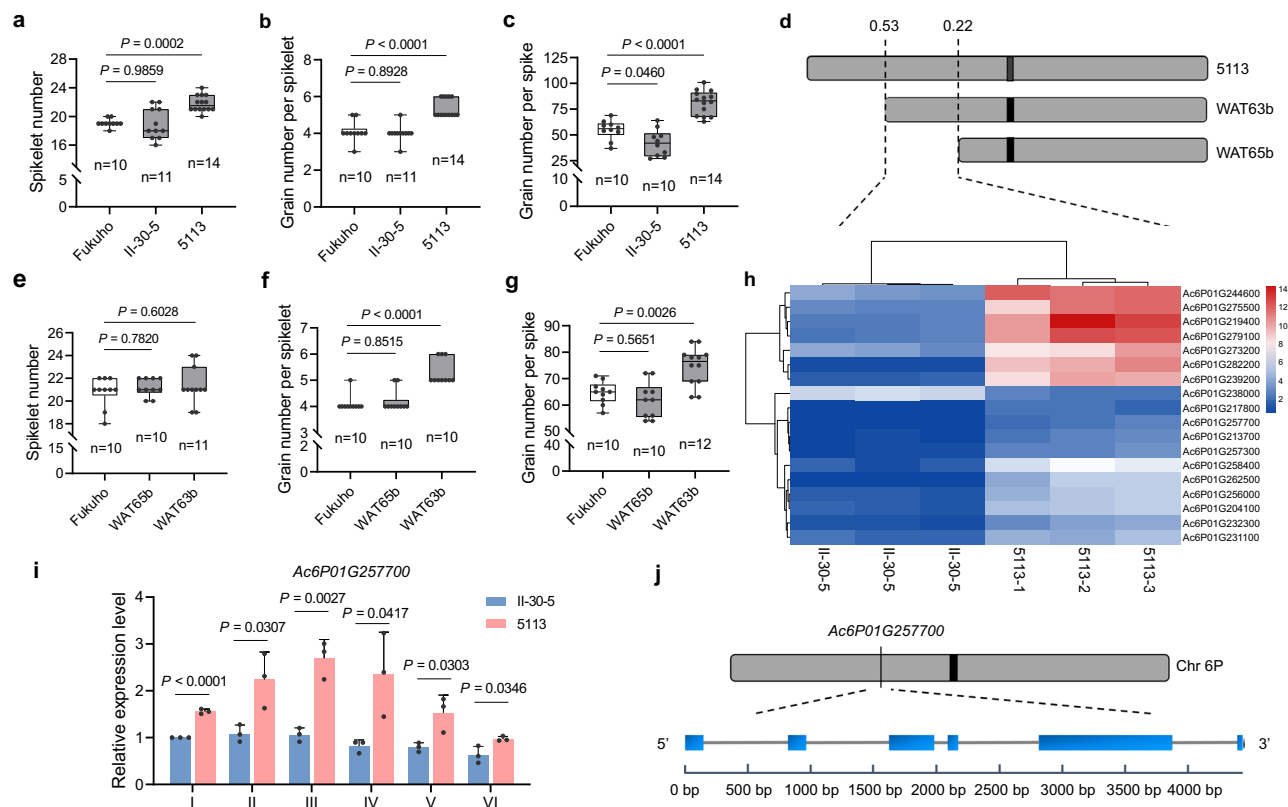


Fig. 1 | Identification of the *AcRRI* gene from *Agropyron cristatum* chromosome 6P. Spikelet number (a), grain number per spikelet (b), and grain number per spike (c) of lines 5113 and II-30-5. d Interval of the *A. cristatum* 6P chromosome containing genes responsible for the high GNS. The gray box represents the 6P chromosome. Spikelet number (e), grain number per spikelet (f), and grain number per spike (g) of lines WAT65b and WAT63b. h Heatmap of a subset of DEGs between the wheat-*A. cristatum* 6P addition lines 5113 and II-30-5 within the interval of 0.22–0.53 on chromosome 6P. i Comparison of the temporal expression of *Ac6P01G257700* in the wheat-*A. cristatum* addition lines 5113 and II-30-5. The different developmental periods represented by Roman numerals are

the single ridge stage (I), double ridge stage (II), floret differentiation stage (III), pistil and stamen formation stage (IV), tetrad stage (V) and three days before heading (VI). j The position and gene structure of *Ac6P01G257700*. The black rectangular box represents the centromere. The blue rectangular boxes represent exons, and the gray lines represent introns. The data are presented as the means \pm S.D.s. In (a–c, e–g) n represents the number of biologically independent plants. Boxes represent the median values and the first and third quartiles; whiskers represent the minimum and maximum values. In (i) $n = 3$ biologically independent replicates. A two-tailed Student's *t* test was used to determine *P* values. Source data are provided as a Source Data file.

AcRRI-OE6 lines were selected for further investigation. Droplet digital PCR (ddPCR) analysis revealed that the lines *AcRRI*-OE1, *AcRRI*-OE3 and *AcRRI*-OE6 contain one, four and two *AcRRI* copies, respectively (Supplementary Data 2). The effects of *AcRRI* were investigated on T_3 transgenic plants at a relatively low seedling density (20 plants per row, 10 cm between plants and 30 cm between rows) in the field. On average, the number of grains per spikelet and GNS of the three transgenic lines were 0.8 and 5.9 more than that of the nontransgenic Fielder (WT), respectively, although the number of spikelets per spike was 1.3 fewer than that of the WT (Fig. 2a–c and Supplementary Fig. 5b–i). Owing to the greater number of fertilized florets at the top and bottom spikelets (Fig. 2c and Supplementary Fig. 5j), the transgenic lines presented more square-shaped spikes than did Fielder (Fig. 2a). The grain yield per plant of the three transgenic lines increased by 3.2 g on average, resulting in a 26.9% increase compared with that of the WT at the lower seedling density (Supplementary Fig. 5k). To further test the effect of *AcRRI* on grain yield, we planted T_4 transgenic lines and their corresponding WT plants at a relatively high seeding rate (270 grains/m²) under normal culture conditions in the field and evaluated their yield. As shown in Fig. 2d–h, the number of grains per spikelet and GNS of the *AcRRI*-overexpressing lines were 0.3 and 4.8 more than that of the WT, resulting in an increase of 9.7% per unit area in grain yield compared with the WT (Fig. 2h and Supplementary Fig. 5l).

To further confirm the effect of *AcRRI* on increasing the yield of elite cultivars, we introduced *AcRRI* into the winter-type common wheat cv. Kenong 199 (KN199), which is driven by the ubiquitin promoter of maize (*AcRRI*-KNOE) and the native *AcRRI* promoter (*AcRRI*-KNCOM), via an *Agrobacterium*-mediated transformation approach (Supplementary Fig. 6a, b). Three *AcRRI*-KNOE lines and two *AcRRI*-KNCOM lines were obtained and used for yield and phenotypic evaluations. At the high seeding rate (270 grains/m²) in the field (Fig. 2i), the average number of grains per spikelet of the T_3 *AcRRI*-KNOE and *AcRRI*-KNCOM lines were 0.3 and 0.2 more, and the average number of GNS were 5.4 and 2.6 more than those of KN199, respectively (Fig. 2j, k). Compared with those of KN199, the yields of the *AcRRI*-KNOE and *AcRRI*-KNCOM lines increased by 12.3% and 9.7%, respectively, per unit area (Fig. 2m). Additionally, no negative effects on other yield-related traits, including thousand-grain weight or effective tiller number, were detected in *AcRRI*-expressing plants (Fig. 2g, l and Supplementary Figs. 5, 6). Based on the above results, we concluded that the ectopic expression of *AcRRI* in common wheat enhances grain yield by increasing the GNS without adversely affecting grain weight or tiller number.

AcRRI* improves floret fertility by activating *TaWOX11-2D

To decipher the molecular function of *AcRRI* in wheat, we performed a spatial expression analysis of *AcRRI* in the addition line 5113 via

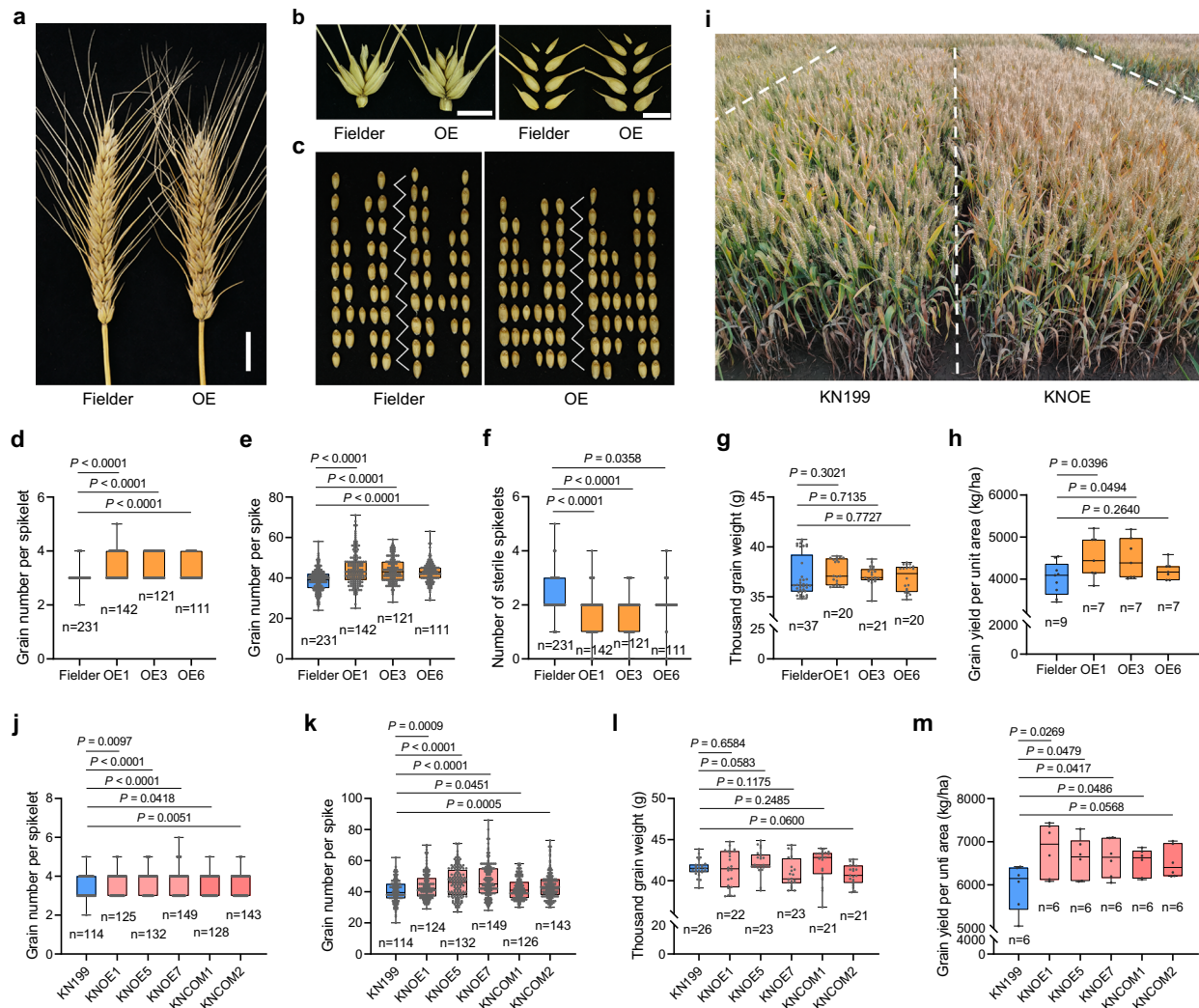


Fig. 2 | *AcRR1* increases the GNS and grain yield of wheat. **a** Spike shapes of the Fielder and *AcRR1*-OE lines. Scale bar, 2 cm. **b** Representative middle spikelet and corresponding disassembled spikelet from the Fielder and *AcRR1*-OE lines. Scale bar, 1 cm. **c** The number of grains along the spike. Grain number per spikelet (**d**), grain number per spike (**e**), number of sterile spikelets (**f**), thousand-grain weight (**g**), and grain yield per unit area (**h**) of the T_4 *AcRR1*-OE lines and the Fielder at a high seeding rate (270 grains/m²) in the field. **i** Assessment of the effect of *AcRR1* on T_3 *AcRR1*-KNOE lines in the field. Grain number per spikelet (**j**), grain number per

spike (**k**), thousand-grain weight (**l**) and grain yield per unit area (**m**) of the T_3 *AcRR1*-KNOE and *AcRR1*-KNCOM lines at a high seeding rate (270 plants/m²) in the field. In (**d**–**h**, **j**–**m**) the data are presented as the means \pm S.D.s. N represents the number of biologically independent plants. Boxes represent the median values and the first and third quartiles; whiskers represent the minimum and maximum values. A two-tailed Student's *t* test was used to determine *P* values. Source data are provided as a Source Data file.

qRT–PCR. As shown in Supplementary Fig. 7a, *AcRR1* transcripts were detected in all examined tissues. However, its expression level was much greater at three days prior to heading than at the floret differentiation stage, especially in the leaves and young spikes.

We subsequently investigated the floret formation of *AcRR1*-OE lines and their WT Fielder by scanning electron microscopy. As shown in Fig. 3a–c, one fewer spikelet was formed in *AcRR1*-OE than in Fielder and no difference in the number of florets per spikelet was detected. These results suggest that the increased grain number per spikelet in *AcRR1*-OE is clearly due to improved floret fertility per spikelet and not to an increased floret number. We subsequently characterized the dynamic expression of *AcRR1* during young spike differentiation in the Pro*AcRR1*:*GUS* line. As shown in Fig. 3d, *AcRR1* was weakly expressed in the differentiating florets, including the floret primordia in the floret differentiation stage (I) and F3–F7 in the pistil and stamen formation stage (II), but was highly expressed in the established florets, including F1–F2 in the pistil and stamen formation stage (II), F1–F3 in the anther connective stage (III) and F2–F4 in the tetrad stage (IV). Notably,

following the differentiation of the floret primordia, the *AcRR1* expression intensity shifted from the basal floret meristem to the middle floret meristem and finally to the apical floret meristem during spike differentiation (Fig. 3d). These results suggest that *AcRR1* may be involved in the regulation of floret fertility.

Cytokinin and auxin indole-3-acetic acid (IAA) are important hormones that affect spike differentiation³⁵. Previous studies have shown that type-B RR proteins are key players in cytokinin signaling^{36,37}, which is highly correlated with stem apical meristem (SAM) development and grain yield^{38,40}. To determine whether the increased grain number per spikelet in the *AcRR1*-OE lines was related to hormone levels, we measured the cytokinin and IAA contents of young spikes from the *AcRR1*-OE lines and Fielder via high-performance liquid chromatography–mass spectrometry (HPLC–MS). The results revealed that the cytokinin trans-zeatin riboside (tZR) significantly accumulated in young spikes of the *AcRR1*-OE line (Fig. 3e), whereas the IAA content did not differ between the *AcRR1*-OE lines and the WT (Fig. 3f).

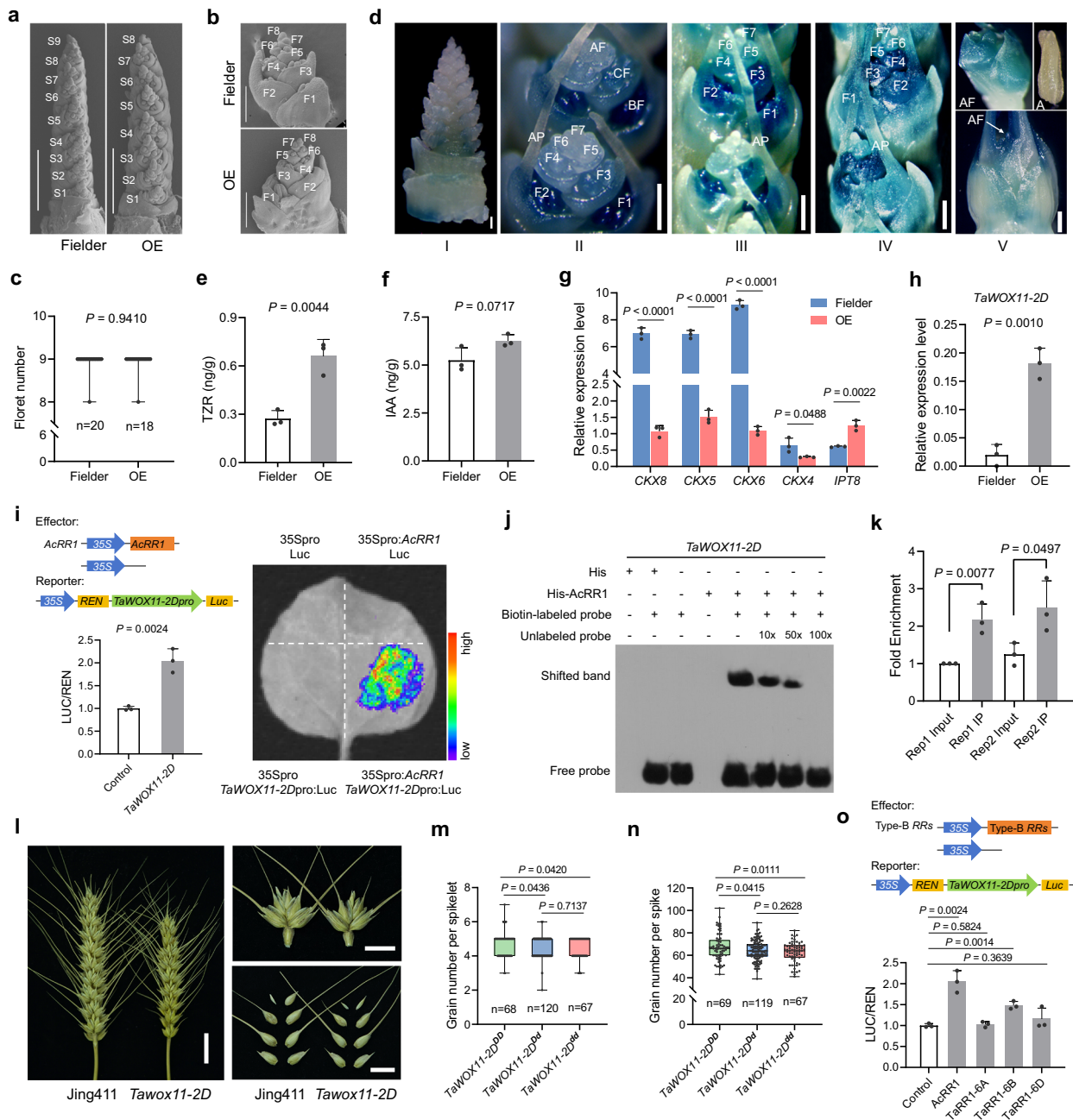


Fig. 3 | *AcRR1* improves floret fertility by activating *TaWOX11-2D*. SEM image of young spikes (a) and central florets (b) from Fielder and *AcRR1*-OE at the pistil and stamen formation stages. Scale bar, a 1 mm; b 0.5 mm. c Comparison of the florets number that eventually formed in Fielder and *AcRR1*-OE. d GUS histochemical assays of *ProAcRR1:GUS* during young spike differentiation. I, floret differentiation stage; II, pistil and stamen formation stage; III, anther connective stage; IV, tetrad stage; V, white anther stage. Scale bar, 100 μ m. In (a–d) S, spikelet; F, floret primordia; AP, awn primordia; AF, apical floret; CF, central florets; BF, basal florets; A, anther. e, f Cytokinin and IAA contents of Fielder and *AcRR1*-OE young spikes at the double ridge stage. g DEGs related to cytokinin degradation and biosynthesis in Fielder and *AcRR1*-OE young spikes. h Expression of *TaWOX11-2D* in young spikes of *AcRR1*-OE lines. i Direct binding of *AcRR1* to the *TaWOX11-2D* promoter. j EMSA of

the binding of *AcRR1*-His to the AGATN (A/T/C) motif in the *TaWOX11-2D* promoter. k ChIP–qPCR assay of the binding of *AcRR1* to the *TaWOX11-2D* promoter. l Representative spikes and middle spikelets of Jing 411 and the *Tawox11-2D* mutant. Scale bar, left, 2 cm; right, 1 cm. The grain number per spikelet (m) and grain number per spike (n) of *F₂* *TaWOX11-2D^{pd}*, *TaWOX11-2D^{pd}* and *TaWOX11-2D^{td}* plants derived from a cross of the *Tawox11-2D* mutant with Jing 411. o Direct binding of *AcRR1* and wheat orthologs to the *TaWOX11-2D* promoter. The data are presented as the means \pm S.D.s. In (e–i, k, o) $n = 3$ biologically independent replicates. In (c, m, n) n represents the number of biologically independent plants. A two-tailed Student's *t* test was used to determine *P* values. Source data are provided as a Source Data file.

To investigate the regulatory roles of *AcRR1*, we performed transcriptome analysis of young spikes and leaves of the *AcRR1*-OE line and its WT and analyzed the transcriptional changes in genes (Supplementary Fig. 7b and Supplementary Data 3–7). The Kyoto Encyclopedia of Genes and Genomes (KEGG) enrichment analysis revealed that

the modules for plant hormone signal transduction and zeatin biosynthesis were enriched in the differentially expressed genes (DEGs) of young spikes and leaves from the *AcRR1*-OE line (Supplementary Fig. 7c, d). Among them, the expression levels of cytokinin degradation genes, including *CKX8*, *CKX5*, and *CKX6*, were significantly

downregulated, and the cytokinin synthesis gene *IPT8* was upregulated (Fig. 3g). These results coincided with the trend in the change in the cytokinin content of the spikes and indicate that *AcRR1* is involved in the accumulation of cytokinins in young spikes of wheat, consequently resulting in an increase in the GNS.

Considering that homeodomain genes, which constitute an important gene family, influence inflorescence stem branching and meristem maintenance in the SAM^{41,42}, we screened four upregulated homeodomain genes (*TraesCS4A02G040600*, *TraesCS2D02G100200*, *TraesCS4D02G261600*, and *TraesCS2A02G188500*) for further characterization to identify the downstream targets of *AcRR1* (Fig. 3h and Supplementary Data 5). Dual-luciferase reporter (DLR) assays revealed that *TraesCS2D02G100200* (*TaWOX11-2D*) was strongly activated by *AcRR1* (Fig. 3i), whereas the remaining three genes were weakly activated (Supplementary Fig. 7e–g). An electrophoretic mobility shift assay (EMSA) further confirmed that *AcRR1* could directly bind to the AGATN (A/T/C) motif of the *TaWOX11-2D* promoter and activate its expression (Fig. 3j and Supplementary Fig. 8a, b). Chromatin immunoprecipitation–qPCR (ChIP–qPCR) analysis also demonstrated that *AcRR1* could directly bind to the promoter of *TaWOX11-2D* (Fig. 3k).

To investigate the function of *TaWOX11-2D*, we screened the whole-exome sequencing mutant library of cv. Jing 411 and obtained a homozygous mutant of *TaWOX11-2D* (*Tawox11-2D*), in which a transversion mutation (C to T) occurred at the 94th amino acid, resulting in the conversion of Gln to a premature termination codon (Supplementary Fig. 8c). Compared with Jing 411, the *Tawox11-2D* mutant produced 1.2 fewer spikelet number per spike, 0.4 fewer grain number per spikelet, and 0.4 more sterile spikelet number and decreased the number of GNS by 15.2 grains (Fig. 3l and Supplementary Fig. 8d–f). To further determine the function of *TaWOX11-2D*, an *F*₂ population was generated by crossing the *Tawox11-2D* mutant with Jing 411. Phenotypic characterization in the field revealed that the *F*₂ plants with the *TaWOX11-2D*^{td} genotype produced 0.5 fewer spikelet number per spike and 0.3 fewer grain number per spikelet than did the *F*₂ plants with the *TaWOX11-2D*^{DD} genotype, resulting in a decrease in the number of GNS by 4.4 grains (Fig. 3m, n and Supplementary Fig. 8g). These results indicate that *TaWOX11-2D* is involved in spike differentiation and the GNS.

We then analyzed the expression patterns of cytokinin degradation and biosynthesis genes in the *Tawox11-2D* mutants to test whether their expression changes in *AcRR1*-OE young spikes are related to *TaWOX11-2D*. The results revealed no significant difference in their expression between plants with the *TaWOX11-2D*^{DD} and *TaWOX11-2D*^{td} genotypes (Supplementary Fig. 8h–k), suggesting that *TaWOX11-2D* is not involved in cytokinin accumulation in young spikes of the *AcRR1*-OE lines.

Furthermore, we compared the expression and binding ability of *AcRR1* with those of its wheat orthologs (*TraesCS6A02G146200*, *TraesCS6B02G174400* and *TraesCS6D02G135500*) to confirm that *AcRR1* functions to increase the GNS in wheat. The four genes presented similar expression patterns, but the peak expression of *AcRR1* appeared one stage earlier (at the pistil and stamen formation stage) than those of its wheat orthologs (at the anther quadrant stage) did (Supplementary Fig. 8l), which may be caused by sequence differences in the promoters (Supplementary Fig. 3e). Furthermore, we examined the binding activity of *AcRR1* and its wheat orthologs to its target gene *TaWOX11-2D* and found that the binding ability of *AcRR1* was markedly stronger than those of its wheat orthologs (Fig. 3o), indicating that *AcRR1* may have a greater affinity than its wheat orthologs.

In summary, the ectopic expression of *AcRR1* in common wheat resulted in the marked accumulation of cytokinins in young spikes and the significantly upregulated expression of *TaWOX11-2D*, consequently enhancing floret fertility and producing a greater GNS.

AcRR1 promotes growth and shortens vernalization duration in wheat

In addition to increasing the GNS, the *AcRR1* transgenic lines presented pronounced early heading and maturity in the greenhouse and in the field (Fig. 4a–c and Supplementary Fig. 9). Compared with the WT (Fielder), the *AcRR1*-OE lines headed 2.1–4.1 d earlier (Supplementary Fig. 9a, b) and matured (milk–ripe stage) 4.4 d earlier in the field than the WT (Supplementary Fig. 9c). The early heading phenotype was also observed in the *AcRR1*-KNOE (13.5 d) and *AcRR1*-KNCOM (12.2 d) lines in the greenhouse (Supplementary Fig. 9d) and in the field (2.8 d) (Fig. 4c and Supplementary Fig. 9e, f). Dynamic observations of inflorescence development revealed that inflorescence development in *AcRR1*-OE lines was dramatically accelerated compared with that in Fielder, especially after the double ridge stage (Fig. 4d). To further understand the influence of *AcRR1* on heading, we investigated the heading dates of *AcRR1*-OE lines under long-day (LD) and short-day (SD) conditions. As shown in Supplementary Fig. 10a–d, similar heading dates were recorded under both LD and SD conditions. These results suggest that the early heading phenotype of *AcRR1*-OE lines is independent of the photoperiod.

Considering that KN199 is a winter type wheat, we then examined the heading dates of the *AcRR1*-KNOE and *AcRR1*-KNCOM lines under different vernalization durations. The results revealed that the early heading phenotype of the transgenic lines was more pronounced under incomplete vernalization (0, 1, 2 and 3 weeks) than under complete vernalization (4 weeks) (Fig. 4e and Supplementary Fig. 10e–g). Even under incomplete vernalization conditions (vernalization for one week), *AcRR1*-KNOE lines headed much earlier (63.8 d) than KN199 (80.2 d) with complete vernalization (vernalization for 4 weeks). The growth and development of the *AcRR1*-KNOE and *AcRR1*-KNCOM lines were almost not inhibited under incomplete vernalization conditions, whereas severe inhibition occurred in KN199, which maintained long-term vegetative growth and produced many tillers, with only a few fertile tillers. The phenotypes of the *AcRR1*-KNOE and *AcRR1*-KNCOM lines capable of heading without vernalization were also verified under field conditions when they were sown in April in Beijing (12.5 h day length, 14.9 °C; average precipitation: 11.8 mm; altitude: 43 m) (Fig. 4f). These results indicate that the expression of *AcRR1* in common wheat greatly reduces the demand for low temperatures by winter wheat, shortening the duration of vernalization and promoting growth and development. In addition, we determined the expression levels of several key flowering regulators. Consistent with the phenotype, the expression levels of the flower-enhancing genes *TaVRN-A1*, *TaVRN-B1*, *TaVRT1* and *TaFT-B1* were significantly upregulated in the *AcRR1*-OE and *AcRR1*-KNOE lines compared with the WT, whereas the expression of the flower-suppressing gene *TaVRN2* was markedly downregulated (Fig. 4g and Supplementary Fig. 10h). Under nonvernalization conditions, the expression levels of *TaVRN1*, *TaVRT1* and *TaFT-B1* were significantly lower than those under vernalization conditions, especially *TaFT-B1*, indicating that KN199 could not head normally or needed a longer time to head. Additionally, the expression levels of *TaVRN1* and *TaVRT1* in the transgenic line were significantly greater, and the expression of *TaVRN2* was significantly lower than that in the WT line, indicating that *AcRR1* affected the expression of genes related to the vernalization pathway (Supplementary Fig. 10h). Taken together, these findings indicate that the ectopic expression of *AcRR1* in common wheat promotes spike differentiation and flowering with a low requirement for vernalization.

AcRR1 regulates early heading by targeting the module *TabHLH25-5B-TaFTs*

To identify the target genes of *AcRR1* associated with heading date, we performed a ChIP-seq assay using leaves of *AcRR1*-KNOE (*ProUbi:AcRR1-FLAG*) plants expressing the *AcRR1*-FLAG fusion protein at the double ridge stage (Supplementary Fig. 6a). A total of 22,676 putative

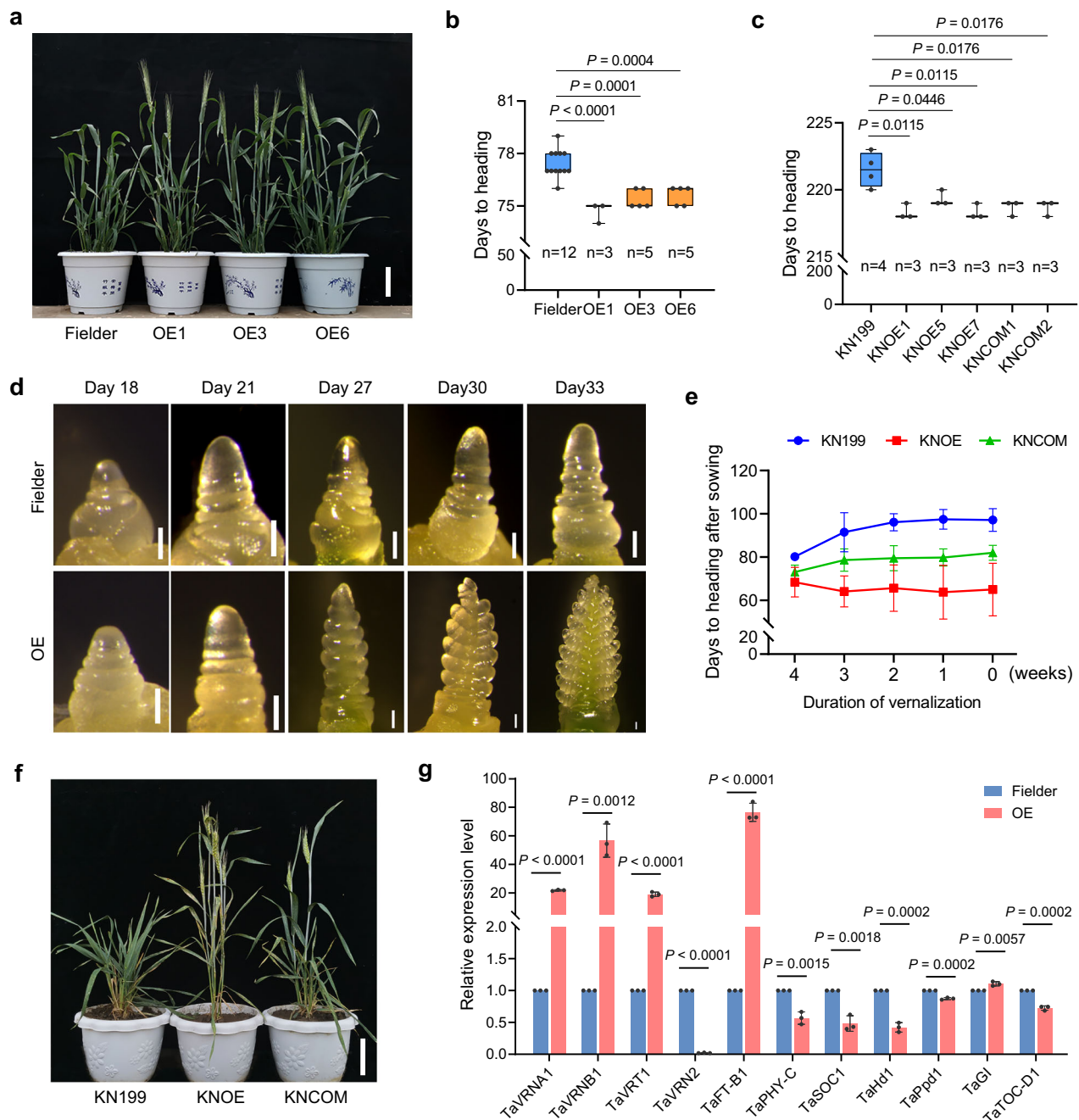


Fig. 4 | *AcRR1* promotes growth and reduces the requirement for the vernalization of winter wheat. **a** Early heading of *AcRR1*-OE lines. Scale bar, 10 cm. **b** Days to heading of the Fielder and *AcRR1*-OE lines. **c** Days to heading of the *AcRR1*-KNOE and *AcRR1*-KNCOM lines. **d** Accelerated spike differentiation in *AcRR1*-OE lines. Scale bar, 100 μ m. **e** Days to heading of the *AcRR1*-KNOE and *AcRR1*-KNCOM lines under different vernalization conditions that were calculated after sowing. The figure was drawn using the mean value, SD and n. **f** Heading of the *AcRR1*-KNOE and *AcRR1*-KNCOM lines under spring sowing conditions in the field. Scale bar, 10 cm.

g qRT-PCR analysis of flowering regulators in Fielder and *AcRR1*-OE leaves at the double ridge stage. The data are presented as the means \pm S.D.s. In (**b**, **c**), n represents the number of biologically independent replicates. In (**g**), n = 3 biologically independent replicates. Boxes represent the median values and the first and third quartiles; whiskers represent the minimum and maximum values. A two-tailed Student's *t* test was used to determine *P* values. Source data are provided as a Source Data file.

AcRR1-binding sites were identified when the cleaned reads were mapped to the Chinese Spring wheat genome, of which 59.57% were localized to genic regions and 40.43% to intergenic regions (Fig. 5a). After annotation, 772 genes were identified as putative AcRR1-bound targets (Supplementary Data 8). KEGG enrichment analysis revealed that the AcRR1 targets were significantly enriched in carbon metabolism, fatty acid metabolism, photosynthesis, and oxidative phosphorylation (Supplementary Fig. 11a, b and Supplementary Data 9). To

obtain high-confidence target genes of AcRR1, we analyzed the DEGs in leaves and young spikes in the *AcRR1*-OE line and Fielder (as determined by RNA-seq) (Fig. 5b and Supplementary Fig. 7b) and extracted the DEGs associated with AcRR1-binding peaks. Using this approach, 46 genes were identified as high-confidence AcRR1 targets (Fig. 5b and Supplementary Data 10). Among these genes, only eight were differentially expressed in young spikes (Fig. 5b and Supplementary Data 10), including the basic helix-loop-helix (bHLH) TF *TabHLH25-5B*

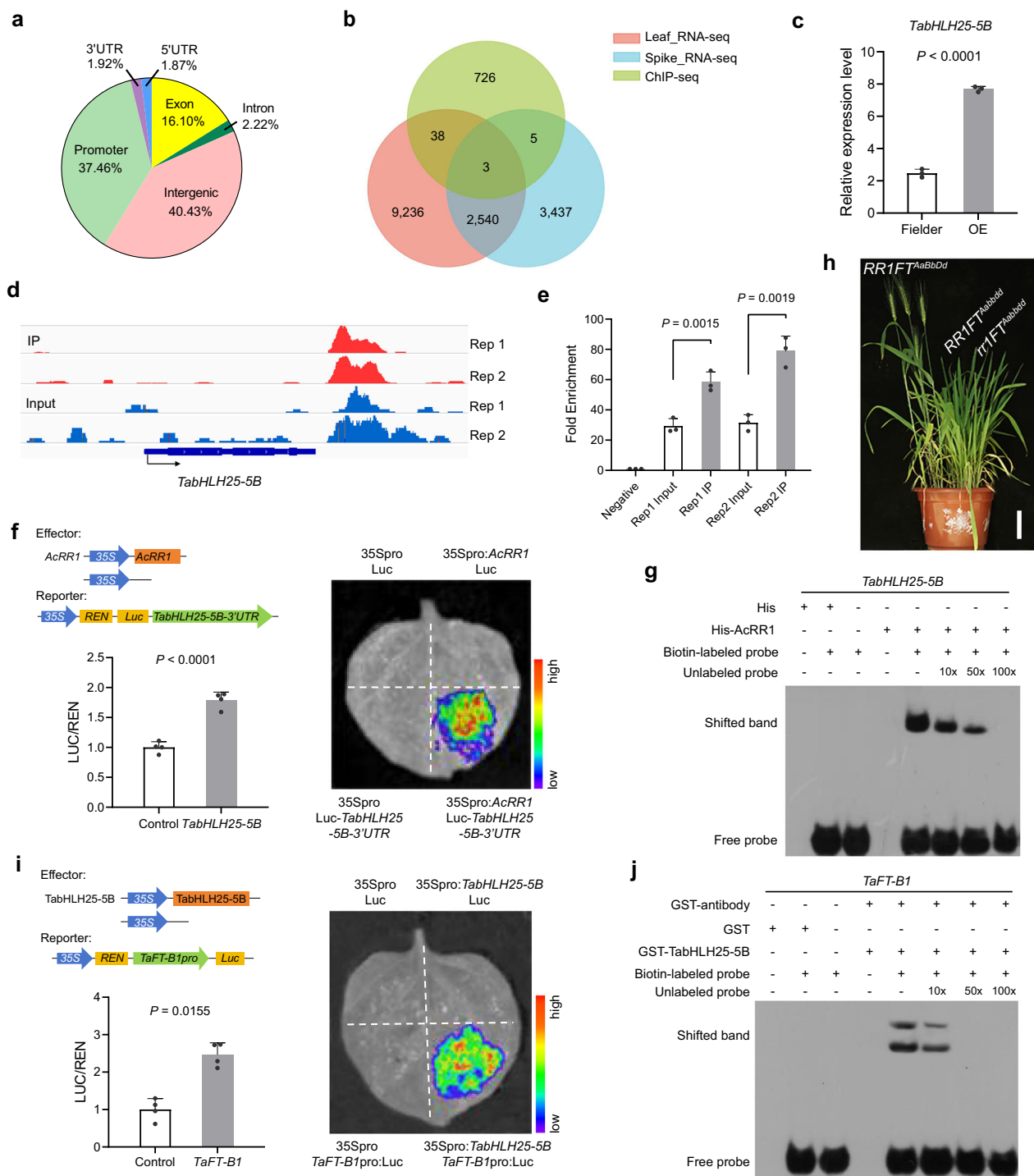


Fig. 5 | AcRR1 promotes early heading by regulating the *TabHLH25-SB-TaFT-B1* pathway. **a Distribution of candidate AcRR1-binding regions across the wheat genome, as determined by ChIP-seq. **b** Venn diagram showing the overlap of the 772 genes bound by AcRR1 with the DEGs identified by RNA-seq of the young spikes and leaves. **c** Expression of *TabHLH25-SB* in *AcRR1*-OE lines. **d** Peak distribution of AcRR1-binding sites for *TabHLH25-SB*. **e** ChIP-qPCR assay of the binding of AcRR1 to *TabHLH25-SB* 3'UTR according to the DLR assay. **f** Direct binding of AcRR1 to the *TabHLH25-SB* 3'UTR according to the DLR assay. **g** EMSA of the binding of AcRR1-His to the**

TabHLH25-SB 3'UTR. **h** Comparison of the heading date of F_2 plants derived from a cross between the *AcRR1*-OE line and the *Taft* mutant. Scale bar, 10 cm. **i** Direct binding of *TabHLH25-SB* to the *TaFT-B1* promoter, as analyzed by the DLR assay. **j** EMSA of the binding of *TabHLH25-SB*-GST to the E-box in the *TaFT-B1* promoter. The data are presented as the means \pm S.D.s. In (**c**, **e**), $n = 3$ biologically independent replicates. In (**f**, **i**), $n = 4$ biologically independent replicates. A two-tailed Student's t test was used to determine P values. Source data are provided as a Source Data file.

(*TraesCS5B03G1260900/TraesCSU02G075200*), whose expression was upregulated in *AcRR1*-OE lines compared with Fielder (Fig. 5c, d).

We performed a ChIP-qPCR assay to verify whether *TabHLH25-SB* is the target gene of AcRR1. The results revealed that AcRR1 could directly bind to the 3'UTR of *TabHLH25-SB* (Fig. 5e). DLR assays

further confirmed that AcRR1 could activate *TabHLH25-SB* expression (Fig. 5f). Moreover, we performed EMSAs and verified that AcRR1 could bind to short sequences containing the AGATN (A/T/C) motif (Fig. 5g and Supplementary Fig. 11c). To investigate the function of *TabHLH25-SB*, we screened and identified two mutants, *Tabhlh25-SB-1*

and *TabHLH25-5B-3*, from the whole-exome sequencing mutant library of Jing 411. *TabHLH25-5B-1* contains a transversion mutation (G to A) at the first AA position of TabHLH25-5B, resulting in the loss of its start codon, whereas the 87th AA of TabHLH25-5B in *TabHLH25-5B-3* is mutated from Trp to a premature termination codon (Supplementary Fig. 11d). The mutants *TabHLH25-5B-1* and *TabHLH25-5B-3* headed 9.4 d and 5.4 d later, respectively, than Jing 411 did in the greenhouse (Supplementary Fig. 11e, f). We further verified the function of *TabHLH25-5B* in the field. In the segregating population isolated from the heterozygous mutants *TabHLH25-5B-1* and *TabHLH25-5B-3*, the plants with the *TabHLH25-5B^{bb}* genotype headed significantly later than did the plants with the *TabHLH25-5B^{BB}* genotype (2.7–4.6 d) (Supplementary Fig. 11g, h). These results indicate that *TabHLH25-5B* is involved in the positive regulation of wheat heading and maturity.

Previous studies have shown that *TaFTs* are the major genes regulating wheat flowering^{43–46}. The ectopic expression of *AcRR1* drastically upregulated the expression (>70-fold) of *TaFTs* (Fig. 4g). To determine the regulatory relationship between *AcRR1* and *TaFTs*, an F₂ population was generated by crossing the *AcRR1*-OE line with the genome-edited *Taft* (*FT^{Aabbdd}*) mutant, which has obviously delayed development and heading (Supplementary Fig. 12a–d). The F₂ plants, regardless of the *RRFT^{Aabbdd}* or *rrFT^{Aabbdd}* genotype, presented a delayed heading phenotype similar to that of the *Taft* mutant (Fig. 5h and Supplementary Fig. 12c). These results indicate that the *AcRR1*-promoted early heading phenotypes in *AcRR1*-OE, *AcRR1*-KNOE and *AcRR1*-KNCOM are dependent on *TaFTs*. Because the distribution of E-box (CANNTG) motifs that can be specifically bound by bHLH TFs⁴⁷ in the promoters of the three homologous genes (*TaFT-A1*, *TaFT-B1* and *TaFT-D1*) is highly consistent and *TaFT-B1* (*TraesCS7B02G013100*) had the highest expression in the *AcRR1*-OE lines (Supplementary Fig. 12e, f), we selected *TaFT-B1* as a representative of the three *TaFT* genes for subsequent analyses. DLR assays and ChIP-seq analyses revealed that the expression of *TaFT-B1* was not directly regulated by *AcRR1* (Supplementary Fig. 12g). Therefore, we hypothesized that *AcRR1* regulated *TaFT-B1* through *TabHLH25-5B*. We performed a DLR assay to confirm this hypothesis and verified that *TabHLH25-5B* could indeed activate the expression of *TaFTs* by binding to their promoters (Fig. 5i and Supplementary Fig. 12h). EMSAs further revealed that *TabHLH25-5B* specifically recognized probes containing E-box (CANNTG) motifs in the *TaFT-B1* promoter (Fig. 5j and Supplementary Fig. 12i, j). These results demonstrated that the ectopic expression of *AcRR1* in common wheat enhances *TabHLH25-5B* expression, which then activates/enhances the expression of *TaFTs*. The *AcRR1*-*TabHLH25-5B*-*TaFTs* pathway identified in this study regulates wheat spike differentiation, resulting in early heading and maturity.

Discussion

Distant hybridization between crops and their relatives is widely used to introduce desirable alien genes and increase genetic diversity for crop improvement. The utilization of wild relatives in wheat improvement remains at the level of cytogenetic analyses and translocation line development; genes cloned from wild relatives, such as *Fhb7*⁴⁸ and *Pm21*⁴⁹, are related mainly to disease resistance. In this study, we introduced *AcRR1*, a type-B RR gene from *A. cristatum*, into common wheat and confirmed that it has pleiotropic effects on increasing the GNS, shortening vernalization duration, and early heading and maturity in wheat. Interestingly, the pleiotropic effect of *AcRR1* was observed only in the *AcRR1*-transgenic lines and not in its donor translocation line WAT63b, implying that some unknown genes on the translocated chromatin repress the effects of *AcRR1* on earlier heading and maturity. The GNS of the WAT63b translocation line increased by 10.0 grains, whereas increases of 2.6–5.9 grains were detected in the *AcRR1*-transgenic lines. This difference can be explained by the different genetic

backgrounds used to generate the translocation and transgenic lines or the presence of unknown gene(s) in the 0.22–0.53 bin of WAT63b, which also functions in spike differentiation in addition to *AcRR1*. Similarly, the *AcRR1* sequences (promotor + CDS) between wheat–*A. cristatum* addition lines 5113 and II-30-5 were identical, but their expression in line 5113 was much greater than that in line II-30-5 (Fig. 1i). The difference in the expression of *AcRR1* between lines 5113 and II-30-5 may be caused by remote regulation, gene interactions or epigenetic modifications.

Cytokinin signaling and the roles of type-B RRs are well studied in model plants; however, little is known about their roles in wheat and its wild relatives. Here, we exploited an ectopic expression approach to characterize the functional roles of *A. cristatum* *AcRR1* in wheat and revealed its positive pleiotropic effects on wheat yield and growth. In *Arabidopsis*, ectopic expression of type-B RRs affects diverse cytokinin-mediated physiological responses, including hypocotyl and root growth, cell number and size in leaves, and shoot initiation^{50,51}. In rice, type-B RRs function in leaf and root growth, inflorescence architecture, anther development, fertilization and trichome formation^{38,52,53}. Disruption of rice *RR21/22/23* resulted in a smaller panicle due to reductions in both primary and secondary branch production³⁸. Although both rice and wheat produce inflorescences, the architecture of their inflorescences is different and arises from differences in the development of their inflorescence meristems⁵⁴. *AcRR1* increased the GNS by increasing the grain number per spikelet and was accompanied by a decreased spikelet number, which is different from the regulation of inflorescence structure by rice type-B RRs. The rice type-B RR mutants presented significantly reduced fertility, which was due mainly to defects in anther and stigma development^{38,53}. Here, *AcRR1* functions mainly in preventing floret abortion and increasing of floret fertility. However, whether *AcRR1* affects wheat floret fertility by regulating anther or pistil development remains unclear. The cytokinin level affects shoot apical meristem (SAM) size and activity and subsequently affects plant panicle branches in rice⁵⁵. A reduced cytokinin level results in failure to maintain meristematic cells in inflorescence meristems, including stamen and pistil primordia³⁷. *AcRR1* overexpression also caused elevated cytokinin levels in young wheat spikes. Therefore, we speculate that *AcRR1* may regulate wheat fertility and inflorescence development by regulating both anther and pistil development, which needs to be confirmed in more detailed experiments. In addition to affecting spike differentiation, *AcRR1* also promotes early flowering. *Ehd1*, a type-B RR in rice that promotes flowering under SD, is much different from *AcRR1* in terms of its sequence and conserved domains⁵⁶. Our results suggest that a functional divergence occurred among *AcRR1* of *A. cristatum* and type-B RRs of *Arabidopsis* and rice.

The GNS can be divided into the spikelet number and the grain number or number of fertile florets per spikelet. A group of genes regulating inflorescence architecture and spikelet development were identified in wheat. Most of these genes, such as the *PHOTOPERIOD RESPONSE* locus (*Ppd-1*)⁵⁷, *FRIZZY PANICLE* (*FZP*)⁵⁸, *TEOSINTE BRANCHED1* (*TB1*)⁵⁹ and the MADS-box genes *VERNALIZATION 1* (*VRN1*), *FRUITFULL 2* (*FUL2*) and *FRUITFULL* (*FUL3*)⁶⁰, increase the spikelet number per spike. They function to increase the spikelet number by delaying the formation of the terminal spikelet and flowering initiation⁶⁰. The grain number per spikelet, which comprises the floret number and floret fertility, is also a major GNS determinant. Enhancing floret fertility is important for increasing the GNS and yield. Mutations in certain genes, such as *Q⁶¹*, *miR172*⁶² and *GN1*⁸, indicate that these three genes are involved in controlling floret number and lateral floret fertility in wheat, but the underlying molecular mechanism remains unknown. Based on the results of this study, we suggest that the increased floret fertility and GNS in *AcRR1*-OE plants can be attributed to the increased cytokinin content and upregulated expression of

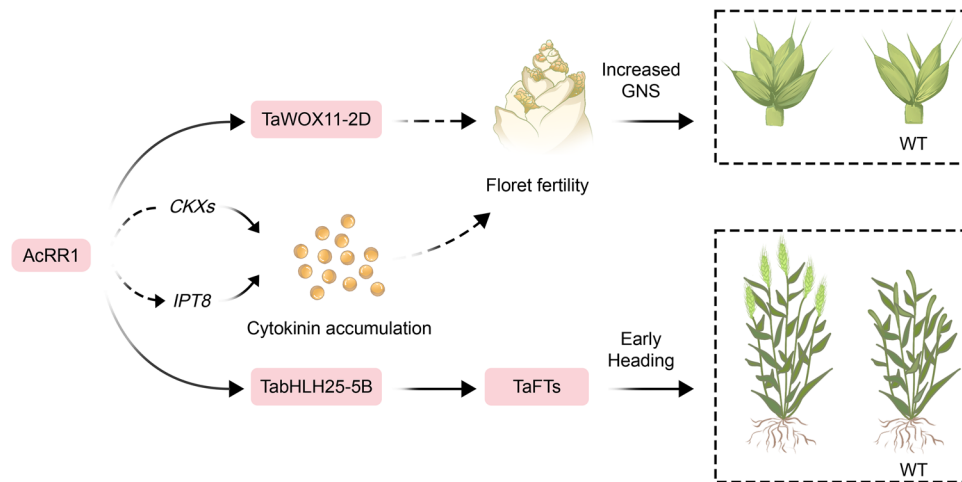


Fig. 6 | Schematic model summarizing the functions of *AcRR1* as a key transcriptional regulator influencing the grain yield and heading date of wheat. The large pleiotropic effects of *AcRR1* elucidated in this work are attributed to the regulation of several sets of target genes. Direct regulation of *TaWOX11-2D* by

AcRR1 and elevated cytokinin levels lead to reduced floret abortion, thus contributing to an increased GNS. Direct regulation of *TabHLH25-5B* by *AcRR1* activates *TaFTs* and confers a pronounced early-heading phenotype. The target genes work together to increase the yield of wheat.

TaWOX11-2D in young spikes. Cytokinins are key drivers of grain yield and control cell division and lateral meristem activity³⁷. In this study, we demonstrated that the *AcRR1*–*TaWOX11-2D* pathway coordinates with cytokinin signals to control floret abortion and accelerate spike differentiation, representing a promising strategy for increasing grain yield.

High yield and early maturity are considered conflicting traits in crop breeding⁶³. Recently, several reports have shown that the trade-off between high yield and early maturity can be uncoupled and even reversed. Overexpression of *NRT1.1A* and *OsDREB1C* in rice resulted in substantial increases in yield and early maturity^{13,64}. In common wheat, constitutive overexpression of *TaCol-BS* increased grain yield and led to earlier heading⁶⁵. Compared with the above pleiotropic genes, *AcRR1* not only eliminates the trade-off between yield and maturity but also shortens the duration of vernalization. Over the past few decades, rising temperatures and hot, dry winds have been identified as critical threats to wheat production^{66–68}. A shortened growth period and the reduced requirement for low temperatures have great potential to reshape wheat fitness to climate change, even without a yield penalty during late sowing⁶⁹, which will benefit farming systems with two harvests per year.

In conclusion, we identified *AcRR1* from *A. cristatum* and revealed its biological functions in controlling wheat floret fertility, vernalization and heading. Based on the results of this study, we propose a functional regulatory model of *AcRR1* (Fig. 6). Ectopic expression of *AcRR1* in common wheat activates *TaWOX11-2D* expression in young spikes, which functions in spikelet meristem (SM) maintenance in the SAM. Moreover, *AcRR1* expression downregulates the expression of cytokinin degradation (*CKXs*) genes and upregulates the cytokinin synthesis gene *IPT8*, resulting in cytokinin accumulation in young spikes. The high expression of *TaWOX11-2D* in conjunction with the accumulation of cytokinins in young spikes results in increased floret fertility, GNS and yield. In addition to the increased GNS, the ectopic expression of *AcRR1* also increases the expression of the transcription factor *TabHLH25-5B*, which then positively regulates the expression of *TaFTs* (major flowering regulatory genes in wheat), consequently promoting spike differentiation and early heading. Notably, the early heading and increased GNS observed in plants expressing *AcRR1* had no negatively coupled effects on grain weight, ultimately increasing grain yield. Overall, the positive roles of the alien gene *AcRR1* from *A. cristatum* provide effective strategies for broadening wheat genetic diversity and improving agronomic traits and grain yield.

Methods

Plant materials and growth conditions

The wheat–*A. cristatum* 6P addition lines 5113³⁰ and II-30-5³¹ were derived from a wide cross between the *A. cristatum* accession Z559 (PPPP, $2n = 4x = 28$) and the *Triticum aestivum* cultivar Fukuho (AABBDD, $2n = 6x = 42$). The wheat–*A. cristatum* 6P translocation lines WAT63b (T6PL-6PS-SBL) and WAT65b (T6PL-6PS-SAS) were developed from wheat–*A. cristatum* 6P addition line 5113 via three generations of backcrossing using the common wheat cultivar Fukuho as the recipient parent. The spring wheat cultivar Fielder and the winter wheat cultivar KN199 were used as the recipients in the transgenic experiments. The *Tawox11-2D*, *Tabhlh25-5B-1* and *Tabhlh25-5B-3* mutants were obtained from the whole-exome sequencing mutant resource of the wheat cultivar Jing 411 and were generously provided by Professor Luxiang Liu, Institute of Crop Science Research, Chinese Academy of Agricultural Sciences. The CRISPR/Cas9 mutant line *Taft* (*FT^{Aabbd}*) used for the analysis of regulatory relationships was kindly provided by Professor Zhongfu Ni, China Agricultural University. All the plants used in this study were cultivated in a greenhouse at 23 °C and 70% relative humidity under a photoperiod of 16 h of light (7:00 a.m.–23:00 p.m.) and 8 h of darkness (23:00 p.m.–7:00 a.m.). The SD conditions included a photoperiod of 10 h of light and 14 h of dark, with the other growth conditions remaining constant. Fukuho, WAT63b, WAT65b, 5113, and II-30-5 plants were grown in the field under normal water and fertilization conditions in Henan Province, and the transgenic wheat and mutants used for field phenotyping were grown in Beijing (116.65°E, 40.13°N), China. For the field experiments conducted at a lower seedling density, the wheat lines were planted in 2 m rows spaced 0.3 m apart. In each row, 20 seeds were sown. For field trials at a relatively high seeding rate (270 grains/m²), a randomized block design with three replicates was used. Each line was sown in a five-row plot, with 260 seeds per row, a 4 m long row and 20 cm between rows.

Phenotypic evaluation under field conditions

The spikelet number, grain number per spikelet, fertile spikelet number, GNS and effective tiller number were determined at maturity for three replicates, with at least 10 randomly selected individuals serving as one replicate. The heading date of the transgenic lines was calculated from the sowing date to the date when approximately 50% of the spikes per line were visible. For yield determination per unit area, approximately 100 plants from each plot were investigated for agronomic traits at maturity, after which all fertile spikes in the plot were

harvested for yield determination using an electronic scale. The percent increase in yield was calculated by subtracting the average grain yield per plant/unit area of the transgenic line from the average grain yield per plant/unit area of the control and dividing it by the grain yield per plant/unit area of the control. The statistical analysis was performed using GraphPad Prism 8 (GraphPad, USA). Differences between the overexpression lines and the control were analyzed using two-tailed Student's *t* tests. $P < 0.05$ were considered significant. The sample size is indicated in the figure legends.

Mapping of *AcRR1*

We used two wheat-*A. cristatum* 6P translocation lines, WAT63b and WAT65b, on the Fukuho common wheat background for genetic analysis to map *AcRR1*. These two lines were subsequently grown in Xinxiang, Henan Province, China, for phenotypic analysis. *AcRR1*-specific primers (Supplementary Fig. 1b and Supplementary Data 11) were used to distinguish WAT63b from WAT65b. Genome resequencing was performed using seedling leaves to further identify the translocated chromosomal segment. A total of 0.2 µg of DNA per sample was used for the DNA library preparations. The sequencing library was generated using an NEBNext® Ultra™ DNA Library Prep Kit for Illumina (NEB, USA) according to the manufacturer's recommendations. The libraries were sequenced by the China Golden Marker Biotechnology Company (Beijing, China) using the Illumina HiSeq 2500 platform with a paired-end read length of 150 bp. Approximately $5 \times$ Illumina short reads were generated. The clean reads were mapped to the genome assembly of *A. cristatum* Z559³² and Chinese Spring RefSeqv2.1³³ via BWA-MEM⁷⁰. The sequencing coverage of reads to the reference genome was calculated with BEDtools⁷¹. The target region was determined by the distribution of coverage of the two translocation lines.

Isolation and bioinformatic analysis of *AcRR1*

The coding sequence (CDS) of the *AcRR1* gene was isolated from *A. cristatum* Z559 cDNA using the *AcRR1*-F/R primers (Supplementary Data 11). The protein sequences of type-B RRs from wheat (*Triticum aestivum* L.), *Aegilops tauschii* L, barley (*Hordeum vulgare* L.), *Brachypodium distachyon* L, *Triticum urartu* L., rice (*Oryza sativa* L.), foxtail millet (*Setaria italica* L.), maize (*Zea mays* L.), *Sorghum bicolor*, *Arabidopsis thaliana*, and soybean (*Glycine max* L.) were downloaded from the Ensembl Plants database (<http://plants.ensembl.org/index.html>). The phylogenetic tree of all the above type-B RRs was constructed via the neighbor-joining method using FastTree software (<https://morgannprice.github.io/fasttree/>). Protein sequences were aligned with MAFFT (Multiple Alignment using Fast Fourier Transform). DNAMAN software (LynnonBiosoft, USA) was used for sequence alignment. Promoter cis-element analysis and candidate binding site prediction were performed using the PlantCARE (<http://bioinformatics.psb.ugent.be/webtools/plantcare/html/>) and JASPAR database.

Subcellular localization

Transient expression assays were performed in wheat protoplasts to determine the subcellular localization of *AcRR1*. The coding sequence of *AcRR1* was subsequently cloned and inserted into the transient expression vector 16318hGFP driven by the CMV 35S promoter. The mCherry signal of the H2B-mCherry fusion protein served as a nuclear signaling marker. Ten-day-old wheat seedling leaves were used for protoplast preparation and the recombinant constructs were introduced into wheat protoplasts via the PEG4000-mediated method⁷². The fluorescence signals were observed using a Zeiss LSM880 laser scanning confocal microscope (Zeiss, Germany).

Transactivation assay in yeast cells

The coding sequence of *AcRR1* was cloned and inserted into the pGBK-T7 vector to generate a pBD-*AcRR1* fusion plasmid. The recombinant

plasmid was transformed into Y2HGold according to the manufacturer's instructions (Clontech). Positive clones were selected on synthetic SD/-Leu-Trp-His medium and incubated at 28 °C for 72 h. Transactivation was further confirmed by X-α-galactosidase staining on SD/-Leu-Trp-His medium.

Genetic transformation of common wheat and phenotypic evaluation

The CDS of *AcRR1* was cloned and inserted into the pCAMBIA3300 vector containing the maize *ubiquitin* (*Ubi*) promoter with *Bam*HI/*Sma*I to generate the Pro*Ubi*:*AcRR1* construct, which was used to generate *AcRR1*-OE lines in the Fielder background. The Pro*Ubi*:*AcRR1*-FLAG and Pro*AcRR1*:*AcRR1*-FLAG constructs driven by the ubiquitin promoter and the 2875 bp sequence upstream of the coding region (the native *AcRR1* promoter) were generated using the same vector backbone and used for the generation of the *AcRR1*-KNOE and *AcRR1*-KNCOM lines on the Kenong 199 (KN199) background. The Pro*AcRR1*:*GUS* construct was the same as the Pro*AcRR1*:*AcRR1* construct, except that the *AcRR1* in Pro*AcRR1*:*AcRR1* was replaced by the GUS reporter gene. The constructs were then transformed into the *Agrobacterium tumefaciens* strain EHA105 (Biomed, China) via the freeze-thaw method according to the product manual. Transformation was performed by infecting immature embryos of Fielder or KN199 using the *Agrobacterium*-mediated transformation method⁷³. Genomic DNAs were extracted using the cetyl trimethylammonium bromide (CTAB) method. The partial sequences for the vector and *AcRR1* were amplified from genomic DNA with specific primers (Supplementary Data 11) to genotype the transgenic plants. The transgenic wheat lines were propagated to the T₂ generation for phenotypic evaluation. More than 20 plants from each line were measured.

RNA extraction and qRT-PCR

The spatial-temporal dynamics and tissue specificity of *AcRR1* expression were determined by qRT-PCR in the wheat-*A. cristatum* 6P addition line 5113. For the analysis of spatial-temporal dynamics, leaf samples were collected at different growth stages from the juvenile period to the filling stage. For the analysis of tissue-specific expression, samples of different tissues were collected at three typical periods: the floret differentiation stage, three days before heading, and the grain-filling stage. For the analysis of the expression of flowering regulators, leaves were harvested 2.5 h after the onset of the day period at the double ridge stage for qRT-PCR, which included approximately 3-week-old seedlings of the *AcRR1*-OE line and 4-week-old seedlings of the *AcRR1*-KNOE line after sowing in the greenhouse. Fresh samples were harvested and quickly frozen in liquid nitrogen. Total RNA was extracted using a plant total RNA extraction kit (ZOMANBIO, China) according to the manufacturer's instructions, and cDNA was generated using a reverse transcriptase kit (ZOMANBIO, China). qPCR was performed using TB Green® Premix Ex Taq™ II (Takara, Japan) in a Step One Plus Real-Time PCR System (Applied Biosystems, USA). Each sample included three replicates. For relative quantification, gene expression was calculated via the 2^{-ΔΔCt} method⁷⁴. Wheat *TaActin* (*TraesCS1B02G024500*) was used as the internal control to calibrate the expression levels of genes. *AcRR1*-specific qRT-PCR primers (Supplementary Fig. 1d, Supplementary Data 11) were used for spatial-temporal dynamics and tissue specificity analyses in wheat.

Western blot analyses

Total protein was extracted from the leaves of one-week-old transgenic plants using a plant total protein extraction kit (Applygen, China) supplemented with a protease inhibitor (Sigma, Germany). After quantification and denaturation, samples of 10 µg protein were separated by SDS-PAGE and transferred to PVDF membranes (Bio-Rad, USA). The membranes were blocked with 5% skim milk in 1× TBST

buffer and incubated with an anti-FLAG antibody (Sigma, 14793S, Germany) at a dilution of 1:1000 at 4 °C overnight. After 3 washes with 1× TBST, the membranes were incubated with the secondary antibody (goat anti-rabbit) (Beyotime, China) at a dilution of 1:10,000. An anti-actin antibody (Sigma, A4080, Germany) at a dilution of 1:1000 was used as a control. After 3 washes with 1× TBST, the membranes were imaged with a chemiluminescence imager device (Tanon, China) after being immersed in an enhanced chemiluminescence (ECL) solution (Beyotime, China).

Droplet digital PCR (ddPCR)

Young leaf tissue was collected for genomic DNA extraction by the CTAB method. A single-copy wheat *TaWaxy* gene in genome D was used as a reference gene⁷⁵. The primer pairs and probe for the *Bar* gene were employed⁷⁶ to determine the transgene copy number in the transgenic wheat plants. The ddPCRs were prepared using ddPCR supermix, digested genomic DNA, *AcRR1*-specific primers and probes (Supplementary Data 11). The reactions were briefly mixed, followed by the addition of droplet generation oil, and then the mixture was placed into a droplet generator for droplet generation. The droplets were transferred to a 96-well PCR plate for PCR amplification. Following PCR, the plate was placed onto a Droplet Digital reader. The data were analyzed using QuantaSoft™ software version 1.3.2 (Bio-Rad).

RNA-seq and data analysis

RNA was extracted from leaves collected from the wheat-*A. cristatum* 6P addition lines 5113 and II-30-5 at the floret differentiation stage. Three biological replicate samples were collected without any treatment. RNA isolation and sequencing were performed by Novogene Co., Ltd. (Beijing, China). Libraries were prepared using the NEBNext® Ultra™ RNA Library Prep Kit (NEB) and then sequenced on an Illumina HiSeq 2500 sequencer. The raw reads from Illumina sequencing were filtered using Trimmomatic⁷⁷ to produce clean reads. The cleaned reads were mapped to the genome assembly of *A. cristatum* Z559³² and Chinese Spring RefSeqv2.1³³ using HISAT2 (v2.0.5)⁷⁸. Deseq2 was used to analyze differential expression⁷⁹. Genes with an adjusted $P < 0.0005$ and absolute fold change (FC) ≥ 0.8 were considered differentially expressed between lines 5113 and II-30-5. Gene Ontology (GO) analysis was performed using the GSeq R package⁸⁰. The KEGG data were analyzed with the Hiplot database (<https://hiplot.com.cn/>). For the overexpression lines, leaves and young spikes were harvested at the double ridge stage, which was approximately 3 weeks after sowing in the greenhouse. RNA isolation and sequencing were performed by Oebiotech Biotech Co, Ltd (Shanghai, China) and Allwegene Tech. Corporation (Beijing, China). Library preparation, sequencing, DEG analysis and enrichment analysis were performed using the same methods described above. An adjusted $P < 0.05$ and absolute FC ≥ 1 were considered to indicate differential expression in the overexpression lines.

Histochemical analysis of GUS activity

Histochemical analysis of GUS activity in Pro*AcRR1*:*GUS* transgenic lines was performed with a GUS staining solution (Solarbio, China) according to the manufacturer's instructions. Briefly, X-Gluc solution (50×) and GUS buffer were thoroughly mixed at a ratio of 1:50 to prepare a 1 × GUS staining solution. The tissues were added to the 1 × GUS staining solution and immersed completely. The samples were incubated at 37 °C for 24 h. As the incubation time increased, blue staining gradually appeared. When the expression level was high, the GUS active site presented blue spots. The samples were soaked in 70% ethanol for 3 h to decolorize the chloroplasts until the negative control was white. The GUS signals were observed under a dissecting microscope and digitally photographed with Image Analysis System 11 software (CRISOPTICAL, China).

Scanning electron microscopy (SEM) analysis

We planted the overexpression lines and controls in the field to observe the process of floret formation. The developing inflorescences were dissected, immediately fixed with 2.5% glutaraldehyde for 48 h, and then dehydrated through a graded ethanol series to absolute ethanol. The samples were subjected to critical point drying with a Leica CPD 030 CO₂ critical point drier (Leica, Germany), mounted on aluminum stubs with double-sided sticky carbon, and then sputter-coated with gold using an SEM coating system (HITACHI, Japan). The samples were then examined with a cold field-emission scanning electron microscope (HITACH, Japan).

Dissection of inflorescences

The *AcRR1*-OE lines and Fielder were grown in a greenhouse, and the growth rates of young spikes were compared. Young spikes of both the *AcRR1*-OE lines and Fielder from the single ridge stage to the floret differentiation stage were isolated using pointed tweezers under a dissecting microscope and then digitally photographed with Image Analysis System 11 software (CRISOPTICAL, China). Stage-specific wheat spikes were classified based on their anatomic and morphological features according to established procedures. At least 5 inflorescences were measured at each developmental stage.

Measurement of endogenous phytohormones

A total of 0.5 g of young spikes was separately collected from *AcRR1*-OE lines and Fielder seedlings at the double ridge stage, with three biological replicates. Cytokinin (tZR) and IAA levels were measured via high-performance liquid chromatography tandem mass spectrometry (HPLC-MS/MS)⁸¹ at Nanjing Ruiyuan Biotech Company. Briefly, fresh samples were frozen in liquid nitrogen and then ground into a fine powder. Ten volumes of an acetonitrile solution and 2 µL of the internal standard mixture were added. The samples were extracted overnight at 4 °C, and then the supernatant was collected after centrifugation at 12,000 × *g* for 5 min at 4 °C. Five volumes of acetonitrile solution were added for secondary extraction. Then, 15–40 mg of CNW C18 QuEChers was added, and the mixture was vigorously shaken for 30 s and centrifuged at 10,000 × *g* for 5 min, after which the supernatant was collected. The elution mixture was dried with nitrogen gas, redissolved in 200 µL of methanol, and filtered through a 0.22 µm organic phase filtration membrane. Separation was achieved on a Poroshell 120 SB-C18 column (150 mm × 2.1 mm, 2.7 µm) with the column temperature set at 30 °C. Phytohormones were detected in positive multiple reaction monitoring (MRM) mode, and the parameters were set as follows: curtain gas, 15 psi; spray voltage, +4500 V, −4000 V; nebulizing gas, 65 psi; and atomization temperature, 400 °C.

Chromatin immunoprecipitation (ChIP) assay

Leaves were sampled from the *AcRR1*-KNOE lines at the double ridge stage for ChIP-seq. KN199 was used as a control for the ChIP assay. A commercial anti-FLAG antibody (Sigma, 14793S, Germany) at a dilution of 1:100 was used for the immunoprecipitation reactions. Two independent biological replicates were performed. ChIP and sequencing were performed by Allwegene Tech. Corporation (Beijing, China). The fragment length of the sheared chromatin was 150 bp. Briefly, 0.5 g of leaves at the double ridge stage were dissected and immediately crosslinked with 1% formaldehyde. Ultrasound was used to shear the genomic DNA into small fragments of a certain length. A specific antibody was added to form an immune complex between the antibody and the target protein. The sample was subsequently decrosslinked, the DNA was purified, and the library was constructed for sequencing. Five nanograms of purified ChIP DNA was used to generate the sequencing library with an NEB kit and was sequenced using the Illumina HiSeq 2500 platform (Illumina, USA). For the ChIP-seq analysis, the raw data were subjected to quality control with FastQC software (<https://www.>

bioinformatics.babraham.ac.uk/projects/fastqc/). The clean reads were aligned to the common wheat reference genome using Bowtie. Sequence alignment map (SAM) files were converted to binary alignment map (BAM) format with SAMtools⁸². The mapped reads were used for peak calling using Model-based Analysis of ChIP-seq V.2 (MACS2)⁸³ with a cutoff q value < 0.05. Peaks were visualized in Integrative Genomics Viewer (IGV) software⁸⁴.

For the ChIP–qPCR analysis, the obtained input genomic DNA and immunoprecipitated (IP) DNA were used as templates for amplification, with deionized water used as the negative control. qPCR was performed under the same experimental conditions as those used for qRT–PCR. The fold-changes were calculated based on the relative enrichment between *AcRR1* and the negative control.

Dual-luciferase reporter (DLR) assay

The CDSs of *AcRR1* and *TabHLH25-5B* were subsequently cloned and inserted into the pCAMBIA1302 vector, and the promoter of *TaFT-B1* was subsequently inserted into the pGreenII 0800-Luc vector. Moreover, the 3'UTR of *TabHLH25-5B* was linked to pGreenII 0800-Luc, followed by luciferase. The constructs were then transformed into the *A. tumefaciens* strain GV3101 (pSoup) (Biomed, China). Positive colonies were grown in Luria-Bertani (LB) medium containing the appropriate antibiotics, collected by centrifugation, and resuspended in infiltration buffer (10 mM MgCl₂, 10 mM MES, and 0.2 mM acetosyringone) at a final OD₆₀₀ = 1.0. The suspensions were mixed in equal volumes and injected into 3-week-old *Nicotiana benthamiana* leaves using a needleless syringe. After infiltration, the plants were cultured first in the dark for 12 h and then with 16 h of light/8 h of dark for 48 h at room temperature. Subsequently, Luc and REN activities were detected using a Dual-Luciferase Reporter Assay System (Promega, USA), and the fluorescence signal was observed with a Night SHADE LB985 charge-coupled device (CCD) imaging apparatus (Berthold Technologies, Germany).

Electrophoretic mobility shift assay (EMSA)

The full-length CDSs of *AcRR1* and *TabHLH25-5B* were inserted into the pET-SUMO and pGEX-6P-1 vectors to express the His-*AcRR1* and GST-*TabHLH25-5B* proteins, respectively. Protein production was induced for 24 h by the addition of isopropyl β-D-1-thiogalactopyranoside (IPTG) at a final concentration of 0.5 mM when the OD₆₀₀ of the cells reached 0.6. Oligonucleotide probes were synthesized and labeled with biotin at the 5' end. The probes were incubated with the nuclear extract at room temperature for 30 min. The entire reaction mixture was loaded onto a 6% native polyacrylamide gel, separated for 1 h at 60 V at 4 °C, and then transferred onto Biotyne® B nylon membranes (Pall Corporation, USA). The signals were visualized with the reagents included in the kit and a ChemiDoc XRS instrument (Bio-Rad).

Genotyping of *Taft* mutants

We crossed the *AcRR1*-OE line with the CRISPR/Cas9-edited mutant line *Taft* (*FT^{Aabbdd}*), in which *TaFT-B1* and *TaFT-D1* were homozygously mutated, and *TaFT-A1* remained heterozygous (homozygous mutation of the three *TaFTs* resulted in no flowering), to examine the relationship between *AcRR1* and *TaFT-B1*. The plants of the F₂ population derived from the cross of the *AcRR1*-OE line and *Taft-B1* mutant were genotyped after harvesting the leaves of each F₂ plant and performing genomic DNA extraction. Each F₂ plant was genotyped by PCR amplification with specific primers for *AcRR1*, *TaFT-A1*, *TaFT-B1* and *TaFT-D1*, and the resulting PCR products were subsequently sequenced.

Statistics and reproducibility

Each experiment was repeated independently at least three times and similar experimental results were obtained. The results from one replicate are shown in the figures. Data are presented in the form of mean ± S.D.s. Means of two samples were compared using Student's

two-tailed t test. GraphPad Prism v9.3.1 and Microsoft Excel 2016 were used for the statistical analyses.

Reporting summary

Further information on research design is available in the Nature Portfolio Reporting Summary linked to this article.

Data availability

All sequence data generated from this study were deposited in the National Center for Biotechnology Information (NCBI): [PRJNA910100](https://www.ncbi.nlm.nih.gov/submit/) for RNA-seq data, [PRJNA911988](https://www.ncbi.nlm.nih.gov/submit/) for ChIP-seq and resequencing data, and [PRJNA906942](https://www.ncbi.nlm.nih.gov/submit/) and [PRJNA1281305](https://www.ncbi.nlm.nih.gov/submit/) for genome sequences and assembly of *A. cristatum* Z559³². Source data are provided with this paper.

References

- Shiferaw, B. et al. Crops that feed the world 10. Past successes and future challenges to the role played by wheat in global food security. *Food Secur.* **5**, 291–317 (2013).
- Kuchel, H., Williams, K. J., Langridge, P., Eagles, H. A. & Jefferies, S. P. Genetic dissection of grain yield in bread wheat. I. QTL analysis. *Theor. Appl. Genet.* **115**, 1029–1041 (2007).
- Wolde, G. M., Mascher, M. & Schnurbusch, T. Genetic modification of spikelet arrangement in wheat increases grain number without significantly affecting grain weight. *Mol. Genet. Genom.* **294**, 457–468 (2019).
- Xiao, J. et al. Wheat genomic study for genetic improvement of traits in China. *Sci. China Life Sci.* **65**, 1718–1775 (2022).
- Sakuma, S. & Schnurbusch, T. Of floral fortune: tinkering with the grain yield potential of cereal crops. *N. Phytol.* **225**, 1873–1882 (2020).
- Sreenivasulu, N. & Schnurbusch, T. A genetic playground for enhancing grain number in cereals. *Trends Plant Sci.* **17**, 91–101 (2012).
- Guo, Z. & Schnurbusch, T. Variation of floret fertility in hexaploid wheat revealed by tiller removal. *J. Exp. Bot.* **66**, 5945–5958 (2015).
- Sakuma, S. et al. Unleashing floret fertility in wheat through the mutation of a homeobox gene. *Proc. Natl. Acad. Sci. USA* **116**, 5182–5187 (2019).
- Ferrante, A., Savin, R. & Slafer, G. A. Relationship between fruiting efficiency and grain weight in durum wheat. *Field Crop Res.* **177**, 109–116 (2015).
- Song, X. et al. Targeting a gene regulatory element enhances rice grain yield by decoupling panicle number and size. *Nat. Biotechnol.* **40**, 1403–1411 (2022).
- Wu, B. et al. Suppressing a phosphohydrolase of cytokinin nucleotide enhances grain yield in rice. *Nat. Genet.* **55**, 1381–1389 (2023).
- Li, Y. et al. *OsMADS17* simultaneously increases grain number and grain weight in rice. *Nat. Commun.* **14**, 3098 (2023).
- Wei, S. B. et al. A transcriptional regulator that boosts grain yields and shortens the growth duration of rice. *Science* **377**, 386 (2022).
- Xue, W. et al. Natural variation in *Ghd7* is an important regulator of heading date and yield potential in rice. *Nat. Genet.* **40**, 761–767 (2008).
- Rossi, M., Bermudez, L. & Carrari, F. Crop yield: challenges from a metabolic perspective. *Curr. Opin. Plant Biol.* **25**, 79–89 (2015).
- Gill, B. S., Friebe, B. R. & White, F. F. Alien introgressions represent a rich source of genes for crop improvement. *Proc. Natl. Acad. Sci. USA* **108**, 7657–7658 (2011).
- Friebe, B., Jiang, J., Raupp, W. J., McIntosh, R. A. & Gill, B. S. Characterization of wheat-alien translocations conferring resistance to diseases and pests: current status. *Euphytica* **91**, 59–87 (1996).
- Mujeeb-Kazi, A. et al. Genetic diversity for wheat improvement as a conduit to food security. *Adv. Agron.* **122**, 179–257 (2013).

19. Dewey, D. R. The genomic system of classification as a guide to intergeneric 885 hybridization with the perennial Triticeae. in *Gene Manipulation in Plant Improvement* (Springer, 1984).
20. Dong, Y. S. et al. Desirable characteristics in perennial Triticeae collected in China for wheat improvement. *Hereditas* **116**, 175–178 (1992).
21. Wu, J. et al. The introgression of chromosome 6P specifying for increased numbers of florets and kernels from *Agropyron cristatum* into wheat. *Theor. Appl. Genet.* **114**, 13–20 (2006).
22. Li, H. H. et al. Mapping of novel powdery mildew resistance gene(s) from *Agropyron cristatum* chromosome 2P. *Theor. Appl. Genet.* **130**, 109–121 (2017).
23. Sun, Y. et al. Identification and fine mapping of alien fragments associated with enhanced grain weight from *Agropyron cristatum* chromosome 7P in common wheat backgrounds. *Theor. Appl. Genet.* **134**, 3759–3772 (2021).
24. Li, L., Li, X., Li, P., Dong, Y. & Zhao, G. Establishment of wheat-*Agropyron cristatum* alien addition lines. I. Cytology of F₃, F₂BC₁, BC₄, and BC₃F₁ progenies. *Acta Genet. Sin.* **24**, 154–159 (1997).
25. Wang, X. et al. Introgression of chromosome 1P from *Agropyron cristatum* reduces leaf size and plant height to improve the plant architecture of common wheat. *Theor. Appl. Genet.* **135**, 1951–1963 (2022).
26. Pan, C. L. et al. Identification of 5P chromosomes in wheat-*Agropyron cristatum* addition line and analysis of its effect on homologous pairing of wheat chromosomes. *Front. Plant Sci.* **13**, 844348 (2022).
27. Zhang, J. et al. Introgression of *Agropyron cristatum* 6P chromosome segment into common wheat for enhanced thousand-grain weight and spike length. *Theor. Appl. Genet.* **128**, 1827–1837 (2015).
28. Zhang, J. et al. An intercalary translocation from *Agropyron cristatum* 6P chromosome into common wheat confers enhanced kernel number per spike. *Planta* **244**, 853–864 (2016).
29. Zhang, Z. et al. Deletion mapping and verification of an enhanced-grain number per spike locus from the 6PL chromosome arm of *Agropyron cristatum* in common wheat. *Theor. Appl. Genet.* **132**, 2815–2827 (2019).
30. Li, Q. F. et al. Chromosomal localization of genes conferring desirable agronomic traits from wheat-*Agropyron cristatum* disomic addition line 5113. *PLOS ONE* **11**, e0165957 (2016).
31. Li, Q. F. et al. Characterization, identification and evaluation of a novel wheat-*Agropyron cristatum* (L.) Gaertn. disomic addition line II-30-5. *Genet. Resour. Crop Evol.* **67**, 2213–2223 (2020).
32. Zhou, S. H. et al. *Agropyron cristatum* genome provides a new insight for wheat improvement with wild relatives. Preprint at *bioRxiv*. <https://doi.org/10.1101/2025.06.24.660289> (2025).
33. Zhu, T. et al. Optical maps refine the bread wheat *Triticum aestivum* cv. Chinese Spring genome assembly. *Plant J.* **107**, 303–314 (2021).
34. Yang, W. J. et al. The genomic variation and differentially expressed genes on the 6P chromosomes in wheat-*Agropyron cristatum* addition lines 5113 and II-30-5 confer different desirable traits. *Int. J. Mol. Sci.* **24**, 7056 (2023).
35. Kieber, J. J. & Schaller, G. E. Cytokinin signaling in plant development. *Development* **145**, dev149344 (2018).
36. Kozuka, J. Control of shoot and root meristem function by cytokinin. *Curr. Opin. Plant Biol.* **10**, 442–446 (2007).
37. Ashikari, M. et al. Cytokinin oxidase regulates rice grain production. *Science* **309**, 741–745 (2005).
38. Worthen, J. M. et al. Type-B response regulators of rice play key roles in growth, development and cytokinin signaling. *Development* **13**, 13 (2019).
39. Niu, J. Q. et al. Whole-genome sequencing of diverse wheat accessions uncovers genetic changes during modern breeding in China and the United States. *Plant Cell* **35**, 4199–4216 (2023).
40. Wang, J. et al. Cytokinin signaling activates *WUSCHEL* expression during axillary meristem initiation. *Plant Cell* **29**, 1373–1387 (2017).
41. Olsson, A. S., Engstrom, P. & Soderman, E. The homeobox genes *ATHB12* and *ATHB7* encode potential regulators of growth in response to water deficit in *Arabidopsis*. *Plant Mol. Biol.* **55**, 663–677 (2004).
42. Perotti, M. F., Ribone, P. A. & Chan, R. L. Plant transcription factors from the homeodomain-leucine zipper family I. Role in development and stress responses. *IUBMB Life* **69**, 280–289 (2017).
43. Yan, L. et al. The wheat and barley vernalization gene *VRN3* is an orthologue of *FT*. *Proc. Natl. Acad. Sci. USA* **103**, 19581–19586 (2006).
44. Chen, Z. et al. Pleiotropic QTL influencing spikelet number and heading date in common wheat (*Triticum aestivum* L.). *Theor. Appl. Genet.* **133**, 1825–1838 (2020).
45. Nitcher, R., Pearce, S., Tranquilli, G., Zhang, X. & Dubcovsky, J. Effect of the hope *FT-B1* allele on wheat heading time and yield components. *J. Hered.* **105**, 666–675 (2014).
46. Chen, Z. et al. A single nucleotide deletion in the third exon of *FT-D1* increases the spikelet number and delays heading date in wheat (*Triticum aestivum* L.). *Plant Biotechnol. J.* **20**, 920–933 (2022).
47. Li, Y., Wang, H., Li, X., Liang, G. & Yu, D. Two DELLA-interacting proteins bHLH48 and bHLH60 regulate flowering under long-day conditions in *Arabidopsis thaliana*. *J. Exp. Bot.* **68**, 2757–2767 (2017).
48. Wang, H. et al. Horizontal gene transfer of *Fhb7* from fungus underlies *Fusarium* head blight resistance in wheat. *Science* **368**, 844 (2020).
49. Xing, L. et al. *Pm21* from *Haynaldia villosa* encodes a CC-NBS-LRR protein conferring powdery mildew resistance in wheat. *Mol. Plant* **11**, 874–878 (2018).
50. Argyros, R. D. et al. Type B response regulators of *Arabidopsis* play key roles in cytokinin signaling and plant development. *Plant Cell* **20**, 2102–2116 (2008).
51. Xie, M. et al. A B-ARR-mediated cytokinin transcriptional network directs hormone cross-regulation and shoot development. *Nat. Commun.* **9**, 1604 (2018).
52. Yamburenko, M. V. et al. Functional analysis of the rice type-B response regulator RR22. *Front. Plant Sci.* **11**, 577676 (2020).
53. Zhao, T. et al. The OsRR24/LEPTO1 type-B response regulator is essential for the organization of leptotene chromosomes in rice meiosis. *Plant Cell* **30**, 3024–3037 (2018).
54. Gao, X. Q., Wang, N., Wang, X. L. & Zhang, X. S. Architecture of wheat inflorescence: insights from rice. *Trends Plant Sci.* **24**, 802–809 (2019).
55. Gu, B. G. et al. *An-2* encodes a cytokinin synthesis enzyme that regulates awn length and grain production in rice. *Mol. Plant* **8**, 1635–1650 (2015).
56. Doi, K. et al. *Ehd1*, a B-type response regulator in rice, confers short-day promotion of flowering and controls *FT*-like gene expression independently of *Hd1*. *Genes Dev.* **18**, 926–936 (2004).
57. Würschum, T., Rapp, M., Miedaner, T., Longin, C. F. H. & Leiser, W. L. Copy number variation of *Ppd-B1* is the major determinant of heading time in durum wheat. *Bmc Genet* **20**, 64 (2019).
58. Bai, X. et al. Duplication of an upstream silencer of *FZP* increases grain yield in rice. *Nat. Plants* **3**, 885–893 (2017).
59. Dixon, L. E. et al. *TEOSINTE BRANCHED1* regulates inflorescence architecture and development in bread wheat (*Triticum aestivum*). *Plant Cell* **30**, 563–581 (2018).
60. Li, C. et al. Wheat *VRN1*, *FUL2* and *FUL3* play critical and redundant roles in spikelet development and spike determinacy. *Development* **146**, dev175398 (2019).
61. Debernardi, J. M., Greenwood, J. R., Jean Finnegan, E., Jernstedt, J. & Dubcovsky, J. APETALA 2-like genes *AP2L2* and *Q* specify lemma identity and axillary floral meristem development in wheat. *Plant J.* **101**, 171–187 (2020).

62. Debernardi, J. M., Lin, H. Q., Chuck, G., Faris, J. D. & Dubcovsky, J. microRNA172 plays a crucial role in wheat spike morphogenesis and grain threshability. *Development* **144**, 1966–1975 (2017).
63. Fang, J. et al. *Ef-cd* locus shortens rice maturity duration without yield penalty. *Proc. Natl. Acad. Sci. USA* **116**, 18717–18722 (2019).
64. Wang, W. et al. Expression of the nitrate transporter gene *OsNRT1.1A/OsNPF6.3* confers high yield and early maturation in rice. *Plant Cell* **30**, 638–651 (2018).
65. Zhang, X. et al. *TaCol-B5* modifies spike architecture and enhances grain yield in wheat. *Science* **376**, 180–183 (2022).
66. Lobell, D. B., Schlenker, W. & Costa-Roberts, J. Climate trends and global crop production since 1980. *Science* **333**, 616–620 (2011).
67. Zhang, T. et al. Climate change may outpace current wheat breeding yield improvements in North America. *Nat. Commun.* **13**, 5591 (2022).
68. Zhao, H. et al. U.S. winter wheat yield loss attributed to compound hot-dry-windy events. *Nat. Commun.* **13**, 7233 (2022).
69. Zabel, F. et al. Large potential for crop production adaptation depends on available future varieties. *Glob. Change Biol.* **27**, 3870–3882 (2021).
70. Oliva, A., Tobler, R., Llamas, B. & Souilmi, Y. Additional evaluations show that specific *BWA-aln* settings still outperform *BWA-mem* for ancient DNA data alignment. *Ecol. Evol.* **11**, 18743–18748 (2021).
71. Quinlan, A. R. & Hall, I. M. BEDTools: a flexible suite of utilities for comparing genomic features. *Bioinformatics* **26**, 841–842 (2010).
72. He, G. et al. Drought-responsive WRKY transcription factor genes *TaWRKY1* and *TaWRKY33* from wheat confer drought and/or heat resistance in *Arabidopsis*. *BMC Plant Biol.* **16**, 116 (2016).
73. Wang, K., Liu, H., Du, L. & Ye, X. Generation of marker-free transgenic hexaploid wheat via an *Agrobacterium*-mediated co-transformation strategy in commercial Chinese wheat varieties. *Plant Biotechnol. J.* **15**, 614–623 (2017).
74. Vandesompele, J. et al. Accurate normalization of real-time quantitative RT-PCR data by geometric averaging of multiple internal control genes. *Genome Biol.* **3**, RESEARCH0034 (2002).
75. Paternò, A. et al. In-house validation and comparison of two wheat (*Triticum aestivum*) taxon-specific real-time PCR methods for GMO quantification supported by droplet digital PCR. *Food Anal. Methods* **11**, 1281–1290 (2018).
76. Wang, K. et al. The gene *TaWOX5* overcomes genotype dependency in wheat genetic transformation. *Nat. Plants* **8**, 110–117 (2022).
77. Bolger, A. M., Lohse, M. & Usadel, B. Trimmomatic: a flexible trimmer for Illumina sequence data. *Bioinformatics* **30**, 2114–2120 (2014).
78. Pertea, M., Kim, D., Pertea, G. M., Leek, J. T. & Salzberg, S. L. Transcript-level expression analysis of RNA-seq experiments with HISAT, StringTie and Ballgown. *Nat. Protoc.* **11**, 1650–1667 (2016).
79. Love, M. I., Huber, W. & Anders, S. Moderated estimation of fold change and dispersion for RNA-seq data with DESeq2. *Genome Biol.* **15**, 550 (2014).
80. Young, M. D., Wakefield, M. J., Smyth, G. K. & Oshlack, A. Gene ontology analysis for RNA-seq: accounting for selection bias. *Genome Biol.* **11**, R14 (2010).
81. Almeida-Trapp, M. & Mithofer, A. Quantification of phytohormones by HPLC-MS/MS including phytoplasma-infected plants. *Methods Mol. Biol.* **1875**, 345–358 (2019).
82. Li, H. et al. The sequence alignment/map format and SAMtools. *Bioinformatics* **25**, 2078–2079 (2009).
83. Gaspar, J. M. Improved peak-calling with MACS2. *Cold Spring Harbor Laboratory* 496521 <https://doi.org/10.1101/496521> (2018).
84. Thorvaldsdottir, H., Robinson, J. T. & Mesirov, J. P. Integrative Genomics Viewer (IGV): high-performance genomics data visualization and exploration. *Brief. Bioinform.* **14**, 178–192 (2013).

Acknowledgements

We thank Zhongfu Ni (China Agricultural University) for kindly providing the *Taft* mutant, Luxiang Liu (Chinese Academy of Agricultural Sciences) for kindly providing the Jing 411 mutants, and Youzhi Ma (Chinese Academy of Agricultural Sciences) for planting the transgenic plants. We also thank Zhiyong Liu (Chinese Academy of Sciences), Kang Chong (Chinese Academy of Sciences), Wenbin Zhou (Chinese Academy of Agricultural Sciences), Hongning Tong (Chinese Academy of Agricultural Sciences) and Yunbi Xu (Chinese Academy of Agricultural Sciences) for their guidance in writing the manuscript. This work was supported by the National Key Research and Development Program of China (2021YFD1200605) and the National Natural Science Foundation of China (32171961).

Author contributions

L.L., H.-Q.L., and H.H. conceived and designed this study. W.Y., H.H., and H.M. performed the experiments. X.L., J.Z., S.Z., K.Q., B.G., Y.L., and J.N. performed the data analysis. L.L., X.Y., and X.G. developed the wheat-*A. cristatum* derivatives and performed the phenotyping. W.Y., H.-Q.L., H.H., P.Y., J.N., and L.L. wrote the manuscript with input from all the authors. All the authors discussed and commented on the manuscript.

Competing interests

The authors declare no competing interests.

Additional information

Supplementary information The online version contains supplementary material available at <https://doi.org/10.1038/s41467-025-61917-5>.

Correspondence and requests for materials should be addressed to Haiming Han, Hong-Qing Ling or Lihui Li.

Peer review information *Nature Communications* thanks Jan Šafář, who co-reviewed with Beata StrejčkováThorsten Schnurbusch and the other, anonymous, reviewer(s) for their contribution to the peer review of this work. A peer review file is available.

Reprints and permissions information is available at <http://www.nature.com/reprints>

Publisher's note Springer Nature remains neutral with regard to jurisdictional claims in published maps and institutional affiliations.

Open Access This article is licensed under a Creative Commons Attribution-NonCommercial-NoDerivatives 4.0 International License, which permits any non-commercial use, sharing, distribution and reproduction in any medium or format, as long as you give appropriate credit to the original author(s) and the source, provide a link to the Creative Commons licence, and indicate if you modified the licensed material. You do not have permission under this licence to share adapted material derived from this article or parts of it. The images or other third party material in this article are included in the article's Creative Commons licence, unless indicated otherwise in a credit line to the material. If material is not included in the article's Creative Commons licence and your intended use is not permitted by statutory regulation or exceeds the permitted use, you will need to obtain permission directly from the copyright holder. To view a copy of this licence, visit <http://creativecommons.org/licenses/by-nc-nd/4.0/>.

© The Author(s) 2025